BMC Genomics

RESEARCH Open Access

Genome-wide identification, expression and evolutionary analysis of the *CLC* gene family in *Vigna radiata* L. reveals its roles in salt resistance

Ashwini Talakayala[1], Dhanasekar Divya[2], P. B. Kirti[3] and Isha Sharma[1,4*]

Abstract

Background Vigna radiata (mungbean) is a nutritionally valuable legume crop with notable stress resilience. However, the molecular basis of its salt tolerance remains poorly understood. The Chloride Channel (CLC) protein family, comprising Cl^- channels and Cl^-/H^+ antiporters, plays crucial roles in anion transport and salt stress regulation in plants. Despite their significance, the CLC gene family has not been systematically investigated in mungbean.

Results We performed a genome-wide identification and characterization of *CLC* genes in mungbean. Seven putative *VrCLC* genes were identified through conserved domain searches. Phylogenetic analysis placed VrCLC members in close evolutionary proximity to legume CLCs, particularly from soybean. Motif analysis revealed conserved acidic/basic residues and glutamates essential for Cl^-/H^+ antiport, while structural modelling confirmed canonical α-helical pores, ligand-binding sites, and CLC/CBS domains. Promoter analysis identified multiple hormone (ABREs- Abscisic Acid Responsive Elements, AF1- auxin-responsive factor binding site) and stress-responsive (MBS-MYB binding sites, STRE-stress response elements, ARE-anaerobic responsive element) cis-elements. qRT-PCR expression profiling revealed that under 100 mM NaCl treatment, *VrCLC-b1* (in leaf and root) and *VrCLC-g* (in flower) were upregulated by approximately fourfold, whereas under 200 mM NaCl, *VrCLC-e* showed more than a threefold induction in roots. Chloride accumulation assays showed maximum Cl^- accumulation in leaves and stems, while root nodules and seeds exhibited no significant change under salt stress. These findings suggest that tissue-specific expression among *VrCLC* genes may influence differential chloride distribution patterns in mungbean.

Conclusion This study provides the first comprehensive genome-wide analysis of the *CLC* gene family in mungbean and highlights their potential roles in salt stress adaptation. These findings lay a foundation for future functional validation and provide potential molecular targets for marker-assisted selection and genome editing aimed at improving salinity tolerance in mungbean.

Keywords Mungbean, CLC genes, Chloride transport, Salt stress, Gene expression

*Correspondence:
Isha Sharma
ishashrikhand@gmail.com; ishasharma.cimap@csir.res.in
[1]International Crop Research Institute for Semi-Arid Tropics, Patancheru, Hyderabad 502324, India
[2]Department of Agricultural Education, Sunchon National University, 413 Jungang-Ro, Suncheon, Jeonnam 57922, Republic of Korea
[3]Agri-Biotech Foundation, Hyderabad 500030, India
[4]Present Address-CSIR- Central Institute of Medicinal and Aromatic Plants (CIMAP), Lucknow 226015, India

Background

Salinity is a major abiotic stress that limits plant growth and agricultural productivity, especially in arid and semi-arid regions. Globally, more than 20% of irrigated lands are affected by salt stress, which is projected to increase at the rate of 0.25 to 0.5 million hectares annually due to climate change and unsustainable irrigation practices [1, 2]. Salinity impairs plant growth and development by inducing osmotic stress, ionic toxicity, nutrient imbalance, and oxidative damage, ultimately reducing photosynthesis, water uptake, and yield [3].

Vigna radiata (mungbean) is a short-duration legume crop. It is rich in protein, vitamins, and minerals, contributing significantly to food security and soil fertility through nitrogen fixation [4–6]. However, it is highly sensitive to salinity, particularly during the early seedling stage [3, 4]. Despite its potential yield of 1.8–2.5 t/ha, global productivity remains low (~570–730 kg/ha) due to salinity and other environmental stresses [7]. Under saline conditions, mungbean accumulates toxic ions such as sodium (Na^+) and chloride (Cl^-), which disrupt cellular homeostasis, impair enzyme activity, and hinder the uptake of essential nutrients like potassium (K^+), calcium (Ca^{2+}), and magnesium (Mg^{2+}) [8]. Thus, ion transporters that sustain cytosolic K^+/Na^+ and Cl^-/NO_3^- balance are critical for maintaining ionic equilibrium and enhancing salt stress tolerance.

Chloride (Cl^-), though essential, becomes toxic in excess and is less studied compared to the well-characterised uptake, transport and sequestration of Na^+ [9, 10]. Cl^- does not bind soil particles, remain freely mobile and is readily absorbed by roots, often leading to toxicity [11]. Plants regulate Cl^- through four transporter families as identified in *Arabidopsis*, SLAC/SLAH (slow anion channels), ALMT (aluminum-activated malate transporters), CLC (chloride channels), and CCC (cation–chloride cotransporters) [12]. The CLC family is conserved across bacteria, yeast, animals, and plants [13]. It includes plasma membrane localised Cl^- channels and Cl^-/H^+ antiporters, mostly localized to the intracellular compartments [14] and together they maintain ion homeostasis, vacuolar Cl^-/NO_3^- storage, and pH regulation [15]. Antiporter-type CLCs, couple Cl^- or NO_3^- transport to proton exchange, using the transmembrane H^+ gradient to drive active ion sequestration and pH regulation [16, 17]. In contrast, channel-type CLCs mediate passive anion fluxes along electrochemical gradients without H^+ coupling [18]. *Arabidopsis* has seven CLC genes (*AtCLC-a–g*) involved in nitrate storage, Cl^- sequestration, and stress responses [16, 17]. These are localized to the tonoplast, Golgi, or thylakoids and contain conserved voltage-gated and Cystathionine beta synthase (CBS) regulatory domains [15]. Differential Cl^- transport and compartmentalization mediated by these CLC's is known to contribute to salt tolerance in crops such as soybean, *Lotus corniculatus*, mungbean, and wheat [18–21]. In *Lotus corniculatus,* increased Cl^- transport to aerial parts is associated with salt stress toxicity [22]. In soybean, the vacuolar Cl^-/H^+ antiporter *GmCLC1* restricts shoot Cl^- accumulation and enhances salt tolerance through vacuolar sequestration [23]. Complementarily, studies on *GsCLC-c2* in wild soybean *(G.soja)* hairy roots/composite plants show that manipulating *CLC* expression alters Cl^-/NO_3^- balance and ion partitioning between roots and shoots, reinforcing a role for legume CLCs in salt responses [24]. Previously, we compared the expression of two *CLC* genes (*VrCLC-b2* and *VrCLC-c*) in salt-tolerant and salt-sensitive mungbean varieties, where lower *CLC* expression and reduced Cl^- transport to leaf tissue were associated with salinity tolerance [3]. Despite their known roles in model and crop plants, *CLC* genes remain uncharacterized in mungbean. This is a critical knowledge gap, especially considering mungbean's sensitivity to salinity and the importance of Cl^- regulation in legumes.

To this end, the present study aims to perform a genome-wide identification and characterization of the *CLC* gene family in *Vigna radiata* to elucidate their roles in salinity adaptation. Using an integrative bioinformatics approach, we analyse gene structure, phylogenetic relationships, chromosomal distribution, and conserved motifs. We compare their expression patterns under salt stress using public RNA-seq datasets and in different tissues using qRT-PCR and infer biological roles by analysing co-expression network and functional annotation. This foundational knowledge will contribute to future functional studies and may enable the development of stress-resilient mungbean varieties via crop improvement strategies.

Material and methods

Identification of CLC family genes in mungbean genomes

The CLC domain (PF00654) from the pfam database in Interpro (https://www.ebi.ac.uk/interpro/) was used to identify candidate sequences in the *Vigna radiata* genome (Vradiata_ver6) using default parameters via the Ensembl plants database (https://plants.ensemble.org/Vigna_radiata/Info/Index). In parallel, BLASTp analysis was performed using *Arabidopsis thaliana* AtCLC protein sequences as queries (Table S1), against the target *Vigna radiata* proteomes in Ensembl Plants [25]. Finally, the candidate *VrCLC* genes identified through both HMM-based searches and BLASTp were cross-compared to ensure consistency of the results. All candidate *VrCLC* entries were checked for completeness (full-length open reading frames) and further validated by confirming the presence of the voltage-gated CLC domain using the NCBI Conserved Domain Database

(NCBI-CDD) (https://www.ncbi.nlm.nih.gov/cdd/). Ultimately, seven *VrCLC* genes were identified in mungbean and were named *VrCLCb1* to *VrCLCg* based on their chromosomal location and homology to *Arabidopsis* CLC protein sequences. The protein sequence length, molecular weight (MW), theoretical isoelectric point (pI), of the identified VrCLC proteins were analyzed using the Expert Protein Analysis System (EXPASY) (https://web.expasy.org/compute_pi/) [26]. Subcellular localization of CLC proteins was predicted using WoLF PSORT (https://wolfpsort.hgc.jp/) [27].

Phylogenetic tree analysis of CLC genes of different crops

To delineate the evolutionary relationship of the mungbean *CLC* genes, multiple sequence alignments was performed between mungbean CLC proteins and CLC proteins from rice, soybean, *Arabidopsis*, wheat, cotton, and tomato, using Clustal Omega (https://www.ebi.ac.uk/Tools/msa/clustalo/). The list of all protein sequences used is provided in Table S2. The neighbor-end-joining method (NJ) was used to create a phylogenetic tree with 1000 bootstrap replications using MEGA11 software [28]. The resulting tree was further visualised and modified using iTOL (https://itol.embl.de) [29].

Gene structure analysis and conserved motif discovery

The coding sequences (CDS) and corresponding genomic sequences of all mungbean CLC genes were retrieved from the Ensembl Plants database (https://plants.ensembl.org) (Supplementary Table S1). Gene structure analysis were performed using the Gene Structure Display Server 2 (GSDS2) (http://gsds.cbi.pku.edu.cn) to visualize the exon–intron organization of the *VrCLC* genes. Conserved motifs within the VrCLC proteins were identified using the MEME Suite (https://meme-suite.org/meme/tools/meme), with the maximum number of motifs set to 10 and default parameters for other settings. Additionally, conserved domains within the seven VrCLC proteins were confirmed using the NCBI Conserved Domain Database (CDD) (https://www.ncbi.nlm.nih.gov/Structure/cdd/wrpsb.cgi) [30], and the domain architecture of the VrCLC proteins was visualized using TBtools.

Promoter analysis of mungbean *CLC* genes

To identify the cis-acting regulatory elements in the promoter regions of mungbean *VrCLC* genes, 1500 bp upstream sequences from the start codon of each *VrCLC* gene were extracted from the mungbean genome. Thereafter, these sequences were submitted to PlantCARE database (http://bioinformatics.psb.ugent.be.webtools/plantcare/html/) to predict putative cis-regulatory elements [31].

Chromosomal locations and synteny analysis

To understand the chromosomal distribution of *CLC* genes in the mungbean genomes, the chromosomal positions of the *VrCLC* genes were extracted from the genome sequence and genome annotation downloaded from the Ensemble Plants database. The chromosomal distribution was visualised using MapGene2Chrom web v2. For identification of gene duplication events among the seven *VrCLC* genes, we employed the one step MCscanX module of TB tool software [32]. The ratio of non-synonymous (Ka) to synonymous (Ks) substitutions (Ka/Ks) in duplicated gene pairs was calculated using the Nei and Gojobori (NG) program of the TB tool software [33]. Selection pressure on duplicated genes was inferred based on the Ka/Ks ratio. The Multiple collinearity scan toolkit (MCScanX) in TBtools [34] was used to analyze greengram and four representative species (*Vigna radiata, Arabidopsis thaliana, Glycine max* and *Oryza sativa)* for the synteny between the *CLC* genes [35].

Weighted Gene Co-expression Network Analysis (WGCNA)

RNA-sequencing data from control and 50 mM NaCl treated mungbean samples were downloaded from the NCBI database (https://www.ncbi.nlm.nih.gov/sra) using the Galaxy platform web server [36]. Three replication accessions (SRR20997626, SRR20997627 and SRR20997628) for control samples and (SRR20997623, SRR20997624 and SRR20997625) for treated samples were used for co-expression analysis. All sequences were checked for quality and low-quality and adaptor sequences were removed using FastQC tool [37]. Clean reads were then mapped to the mungbean genome (Vigna_radiata.Vradiata_ver6 version) using the HISAT2 tool on the Galaxy web server [38]. Mapped reads were quantified using FeatureCounts [39], and differential expression analysis was performed with DESeq2 [40]. Fragments per kilobase of transcript per million mapped reads (FPKM) values were calculated. Genes with FPKM ≥ 1 were selected for co-expression analysis of *VrCLC* genes using the iDEP web server with the power of 4 as soft-thresholding value [41]. Cytoscape software was used to visualize the co-expressed *VrCLC* genes (https://cytoscape.org/). The top twenty co-expressed genes were analysed for gene ontology analysis (GO) (Supplementary Table S5) and KEGG pathway analysis using the KOBAS web server (http://kobas.cbi.pku.edu.cn/).

Protein modelling

The seven VrCLC proteins were analysed for their three-dimensional (3D) structure using the online webserver I-TASSER [42]. The 3D structures were generated using the two inbuilt assembly programs of I-TASSER: LOMETS and TASSER. Protein analogs were created for each

protein through multiple threading alignments. The best 3D models were created based on the highest confidence score and homology with structures in the PDB database. The best 3D protein models were further refined using the ModRefiner program [43].The final 3D structures of the seven VrCLC proteins along with their predicted ligand-binding sites were visualized using Discovery Studio v.21.1 software.

Plant material and stress treatment

Seeds of mungbean genotype MGG295 (Madhira Greengram-295) were procured from Agricultural Research Station, Madhira, PJTSAU, Telangana. The experimental setup was carried out at the glass house facility at ICRISAT, Patancheru. Nursery polybag of 5 kg capacity were filled with a soil mixture composed of black soil, sand, and vermicompost in a 1:2:1 ratio. 15 mungbean seeds were sown in each polybag and thinning was done to retain five plants per pot after one week of germination. These plants were maintained under well-watered conditions up to 21 days at 28/20 °C day/night temperatures. Salt treatment was given after expansion of first trifoliate leaf stage (21st days after sowing-DAS). Salinity stress was inflicted at two levels *i.e*., 100 mM and 200 mM NaCl with three replicates for each treatment. Polybags were irrigated with NaCl solution by adding a total volume of 400 ml on alternative days. Two tissue types (root and shoot) were collected at control 0 h (control), 30 min, 3 h, 6 h, 24 h, 48 h, 72 h, 7 d and 10 days, respectively, after salinity treatments. A parallel set of plants was maintained under the same salinity treatments until the reproductive stage. These plants were irrigated with NaCl solutions on alternate days until seed harvest. At 45 days of age, different tissue samples like root, shoot, stem, flower, immature cotyledon (IMC), root nodule (RN), and seeds were collected from both salinity treatments under the same experimental conditions (28/20 °C day/night temperature) with three biological replicates per treatment. All tissue samples were snap-frozen in liquid nitrogen and stored at −80 °C until further analysis.

Chloride ion uptake

Chloride ion (Cl^-) concentrations in root, leaf, stem, flower, IMC, RN, and seed samples were determined titrimetrically following Mohr's method [44]. Briefly, Cl^- was extracted by boiling 0.25 g of dried sample in distilled water, followed by titration with 0.5 N silver nitrate ($AgNO_3$). Potassium chromate was used as an indicator, and the formation of a red-brown silver chromate precipitate marked the titration endpoint.

Quantitative real time PCR validation

Expression anlaysis of identified *VrCLC* genes was conducted in root and shoot tissues in mungbean plants treated with salinity using qRT-PCR. Additionally, upon reaching reproductive maturity, various tissues were analyzed for the expression of 7 *VrCLC* genes under both levels of salinity. We designd qRT-PCR primers using primers Designer Tool (https://www.thermofisher.com). Total RNA was extracted using Trizol method (Nucleospin RNA Plant, Macherey–Nagel, Duren, Germany) from 100 mg of tissue (leaf, root, stem, flower, IMC, RN and seed of mungbean treated with or without NaCl). The purified RNA was converted to cDNA with the iScript™ cDNA synthesis kit, Biorad laboratories, California, United States. Quantitative real time PCR was then performed on a CFX96 Real-Time PCR system (Bio-Rad, USA) using Fast SYBR Green Master Mix (Applied Biosystem, Thermo Fisher Scientific, North America, USA), following the manufacture's protocol. Gene expression levels were calculated using the 2^−ΔΔCt method with Actin as the internal reference, and the resulting relative expression values were $\log_2$-transformed for visualization. Each reaction (10 µl total volume), containing 5 µl of Fast SYBR Green master mix, 0.5 µl of each forward and reverse primers, 1 µl of cDNA template and 3 µl of nuclease free water. The PCR thermal cycler was set as follows: pre-denaturation at 95 °C for 5 min; 40 cycles of 95 °C for 10 s and 60° C for 30 s; the dissociation stage was set as follows: 95 °C for 10 s, 60 °C for 5 s and 95 °C for 5 s. For each condition, three independent biological replicates were analyzed for both shoot and root tissues, with each biological replicate assayed in three technical replicates. For tissue-specific expression profiling (root, shoot, leaf, stem, flower, immature cotyledon, root nodule, and seed), three biological replicates were used, each with three technical replicates. *VrActin* was used as an internal reference gene. Primer sequences are listed in (Supplementary Table S10).

Statistical analyses

All data were analyzed using two-way analysis of variance (ANOVA) and are presented as mean ± SE of three independent replicates. Dunnett's multiple comparison test was performed using GraphPad Prism (version 9.0), and differences between stress treatments were considered significant at $P \leq 0.05$.

Results

Identification of *VrCLC* genes in mungbean

The reference genome sequence and annotation files of *Vigna radiata* (assembly version Vradiata_ver6.0) were retrieved from the Ensembl Plants database (https://plants.ensembl.org) for identification and characterizatio n of CLC genes. To identify *VrCLC* genes in mungbean, the conserved CLC domain (PF00654) was used to search annotated proteins of *V.radiata*. A total of 7 *VrCLC* genes were identified in the genome of *V.radiata*. The CDS and

Table 1 List of the identified CLC family genes in *Vigna radiata*: Characteristics of *Vigna radiata* chloride channel (*VrCLC*) gene family members, including their genomic, proteomic, and predicted subcellular localization features. The table listed shows that the gene name, corresponding gene ID, protein ID, gene length (in base pairs), chromosome location, protein length (number of amino acids), theoretical isoelectric point (pI), and molecular weight (MW, in kilodaltons). Predicted subcellular localization is indicated along with the number of prediction hits for each compartment, including plastid, vacuole, endoplasmic reticulum (E.R.), and Golgi apparatus. Gene IDs and protein IDs are based on the *V. radiata* genome annotation, with chromosome positions. These details provide insight into the structural diversity, chromosomal distribution, and potential functional specialization of VrCLC family proteins

Gene Name	Gene Id	Protein id	Gene Length	Chromosome Position	Amino acid	PI	MW (kDa)	Subcellular localization
VrCLC-b1	LOC106769047 (*Vradi07g07220*)	XP_014509989.1	2349	Chr7	782	8.20	86.64	Plastid: 10; Vacuole:2; E.R:2
VrCLC-b2	NW_014543262 (*Vradi0007s01770*)	NW_014543262.1	2337	Chr 7 scaffold_7	778	8.39	86.11	Plastid: 8; Vacuole:2; E.R:4
VrCLC-c	LOC106771913 (*Vradi01g06410*)	XM_014657961.2	2334	Chr1	777	7.54	85.36	Plastid: 7; Vacuole:7; E.R: 3; Golg:1
VrCLC-d	LOC106777769 (*Vradi11g00590*)	XP_014520999	2361	Chr11	786	7.89	86.72	Plastid:12; E.R:2
VrCLC-e	NW_014542624 (*Vradi0394s00010*)	NW_014542624.1	1962	Chr 3 scaffold_394	653	6.43	70.14	Plastid:10;Vacuole:3; E.R:1
VrCLC-f	LOC106762104 (*Vradi05g22020*)	XP_014501304.1	2007	Chr5	668	6.44	71.59	Plastid:11; Vacuole: 1; E.R:2;
VrCLC-g	LOC106768211 (*Vradi07g20630*)	XP_014508695.1	2301	Chr7	766	8.89	83.98	Plastid: 12; Vacuole: 2

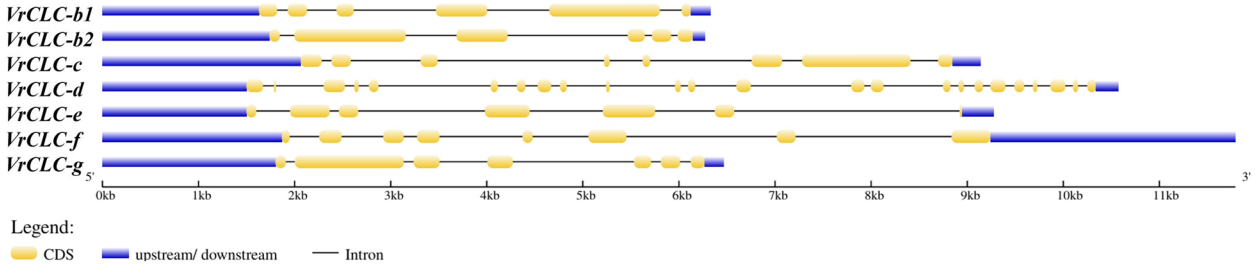

Fig. 1 Gene structures showing the organization of exons and introns of *VrCLC* genes. Gene Structure: Schematic representation of the gene structures of *VrCLC-b1,VrCLC-b2, VrCLC-c, VrCLC-d, VrCLC-e, VrCLC-f,* and *VrCLC-g*. The yellow boxes indicate coding sequences (CDS), blue regions depict upstream/ downstream untranslated regions, and black lines represent introns

the corresponding amino acid sequence lengths of the identified genes were tabulated. The amino acid lengths of *VrCLCb1* to *VrCLCg* ranged from 653 to 786 amino acids. The predicted molecular weight of VrCLC proteins ranged from 83.98 to 86.72. The theoretical pI values ranged from 6.43 to 8.89. Subcellular localization analysis predicted that all VrCLC proteins are located primarily in the plastids and other organelles (Table 1).

Gene structure of *VrCLC* genes in mungbean

The seven *VrCLC* gene family members, labelled as *VrCLC-b1,b2,c,d,e,f* and g exhibit significant structural diversity. They vary considerably in their total gene length, number of exons, size of exons, intron, and extent of untranslated regions (UTRs). *VrCLC-b1* has a total length of approximately 6.5 kb and contains six exon and five intron, *VrCLC-b2* is around 6.2 kb with six exons and five intron, and a well-defined UTR region. *VrCLC-c* is longer with 9.2 kb length with nine exon, eight introns and a relatively shorter downstream UTR. *VrCLC-d* is the largest gene of 11 kb comprising 24 small exons and 24 introns, along with extensive UTRs. *VrCLC-e* spans 8.8 kb and includes seven exons and six introns, having distinct 3' UTR, *VrCLC-f* is approximately 10.5 kb in length, containing ten exons and nine introns, along with a long 3′ UTR. Finally, *VrCLC-g* is about 6.5 kb long, with seven exons, six relatively short introns, and short UTRs (Fig. 1) (Supplementary Table S1).

Phylogenetic analysis and classification of the *VrCLC* gene family

To understand the evolution and subclass differentiation of CLC family proteins in mungbean, a comparative phylogenetic analysis was performed with both monocot and dicot species viz. *Oryza sativa, Solanum lycopersicum, Arabidopsis thaliana, Triticum aestivum, Gossypium hirsutum, Glycine max* and *Vigna radiata.* CLC gene sequences were retrieved from the respective species

databases. A total of 80 CLC protein sequences collected from the seven plant species were used for phylogenetic analysis using MEGA11 software (Fig. 2). The phylogenetic analysis grouped CLC proteins from mungbean and six other plant species into seven distinct clades (CLC-a to CLC-g), consistent with previous classifications in other plants. The seven VrCLC proteins were distributed across six clades, with VrCLC-b1 and VrCLC-b2 forming a duplicate pair in the CLC-b clade, suggesting a gene duplication event. Most VrCLC proteins clustered closely with their orthologs from *G. max*, suggesting the evolutionary proximity between the two legumes, while some also showed close relationships with *S. lycopersicum* and *A. thaliana* proteins. The clustering pattern indicates functional conservation of CLC proteins across species, with mungbean likely retaining a core set of CLC genes similar to other diploid plants (Supplementary Table S2).

Sequence analysis of *VrCLC* gene family

The structural analysis of *VrCLC* genes revealed considerable variation in exon–intron organization, conserved motifs, and protein domains (Fig. 3). The phylogenetic tree (Fig. 3a) showed that *VrCLC-b1* and *VrCLC-b2* are closely related which supports their origin from a duplication event. Exon–intron mapping (Fig. 3b) showed that *VrCLCd* contains the highest number of introns, whereas *VrCLC-b1* and *VrCLC-b2* have the simplest gene structures with the fewest introns. *VrCLC-d* contained the highest number of exons (24), whereas *VrCLC-b1*and *VrCLC-b2* had the fewest (6). Thus, the number of exons in *VrCLC* genes ranged from 6 to 24, with an average of 9.85 exons per gene. Corresponding intron numbers varied from 5 to 23, resulting in an average of 8.85 introns per gene and an average intron-to-exon ratio of approximately 1:1.1. Such variability in exon–intron organization suggests potential diversification in gene regulation and evolutionary trajectory within the *VrCLC* family. Motif analysis (Fig. 3c) identified ten conserved motifs shared among most VrCLC proteins, although VrCLC-e possessed none of the conserved motifs. It could indicate that VrCLC-e might have diverged functionally from other VrCLC proteins, potentially acquiring a specialized or altered role. The sequence logos for all the 10 conserved motifs identified in VrCLC proteins are displayed in Fig. 4. These motifs represent highly conserved

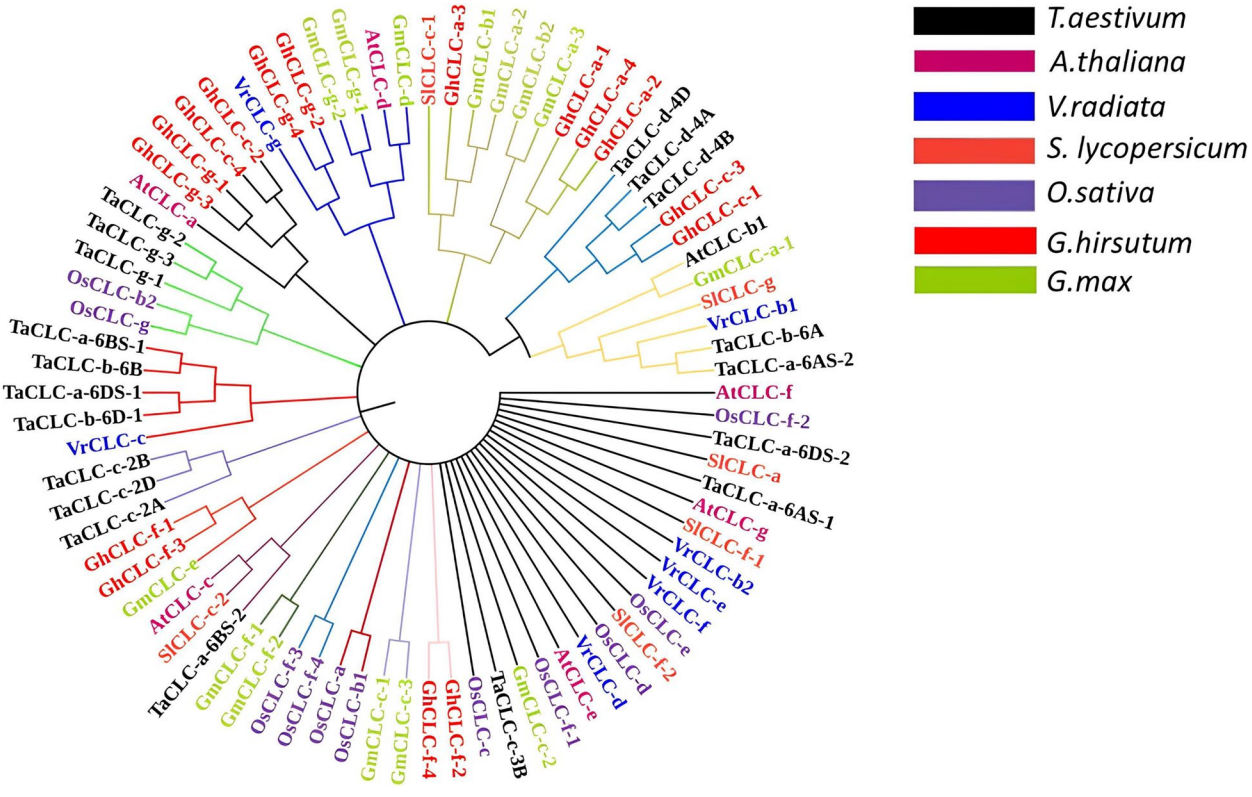

Fig. 2 Phylogenetic trees showing relationships of CLC genes family of *O. sativa, G. max, A. thaliana, S. lycopersicum, G.hirsutum, T.aestivum and V.radiata.* The trees were constructed using muscle alignment method and a bootstrap replicate of 1000. The trees with the highest bootstrap support for each gene class have been shown here. *Triticum aestivum* (black), *Arabidopsis thaliana* (magenta), *Vigna radiata* (blue), *Solanum lycopersicum* (orange), *Oryza sativa* (purple), *Gossypium hirsutum* (red), and *Glycine max* (green). Gene labels use species prefixes (Ta, At, Vr, Sl, Os, Gh, and Gm) followed by the CLC subclass designation (a–g) based on the *Arabidopsis* nomenclature; wheat homeologs are further distinguished by subgenome/chromosome number and form (e.g., 2A/2B/2D, 6A/6B/6D)

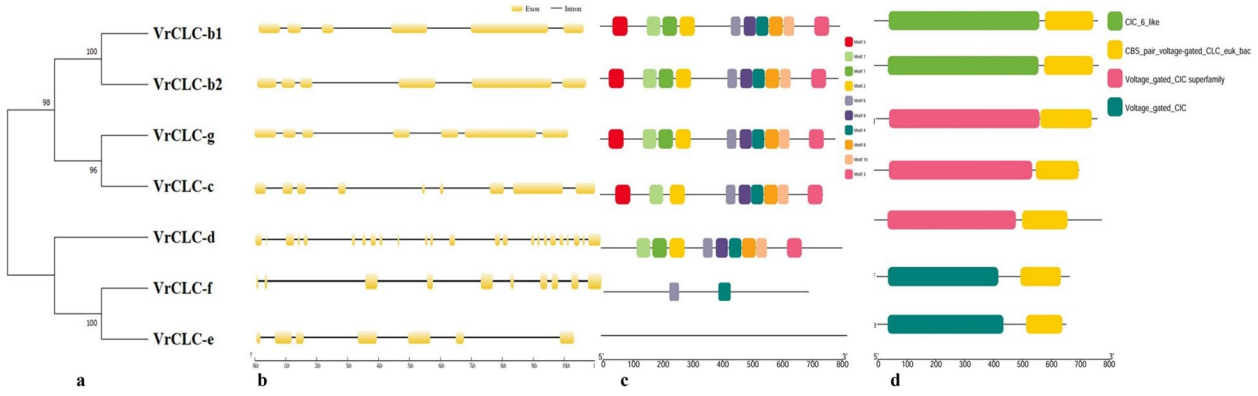

Fig. 3 Phylogenetic relationships, gene characterization-exon intron region, conserved motif analysis of VrCLC proteins and conserved protein domain of CLC genes in *Vigna radiata*.**a** Phylogenetic tree of CLC proteins in *vigna radiata:* The phylogenetic tree was constructed using the neighbor joining method with MEGA 7 and including CLC proteins of *vigna radiata*.**b** Intron–exon structures of the CLC family in *vigna radiata* (a) and partial amino acid sequence alignment of the *VrCLC* family. **c** Distribution of the conserved motifs in mungbean CLC proteins. Ten conserved motifs are marked with different colored boxes. The scale bar indicates 100 aa. **d** Protein conserved domain in CLC genes of *V. radiata*. Green boxes represent the presence of CLC_6 like domain, yellow boxes represent CBS_pair_voltage-gated_CLC_euk_bac domain, pink boxes represent Voltage_gated_ClC superfamily domains while the dark green boxesrepresents the Voltage_gated_ClC, rest of the protein sequences except the conserved domain in the respective VrCLC protein sequences

Fig. 4 Sequence logo of the *VrCLC* conserved motifs. Sequence logos representing conserved motifs in the protein sequences analyzed. Amino acid sequence logos for the ten most conserved motifs identified in the protein/gene family name, e.g., *CLC transporter* were generated using MEME Suite

amino acid patterns characteristic of the voltage-gated chloride channel (ClC) superfamily. The conservation of acidic (E, D) and basic (K, R) residues in several motifs suggests their potential involvement in ion transport and gating, while hydrophobic residues likely contribute to membrane association and structural stability. Domain analysis (Fig. 3d and Supplementary Table S3) revealed that VrCLC proteins contain atleast one of the characteristic voltage-gated ClC domains (Voltage_gated_ClC, ClC_6_like, or CBS pair) representing the core functional domain responsible for chloride ion transport. The overall similarity in motif composition and domain structure among VrCLC proteins within the same clade supports their functional conservation.

Analysis of the promoter cis-elements in the CLC gene family

Promoter analysis of seven *VrCLC* genes (*VrCLC-b1* to *VrCLC-g*) revealed the presence of multiple cis-regulatory elements (CREs) (Fig. 5). These CREs were associated with hormonal responsiveness, stress responses, and other key regulatory functions. Hormone-responsive elements included ABRE (Abscisic Acid Responsive Elements), which were distributed in *VrCLC-c, VrCLC-e,* and *VrCLC-f*, suggesting potential ABA mediated transcriptional regulation. The TGA element, associated with auxin responsiveness, was present in *VrCLC-b1, VrCLC-e* and *VrCLC-f.* In addition, AF1 (auxin-responsive factor binding site) elements were detected in *VrCLC-b1,VrCLC-d,VrCLC-e,VrCLC-f* and *VrCLC-g.* Stress-related cis-elements such as MYB, MBS (MYB binding sites), and MYB recognition elements were found in *VrCLC-b2*, *VrCLC-c*, *VrCLC-d*, *VrCLC-e*, and *VrCLC-g*,

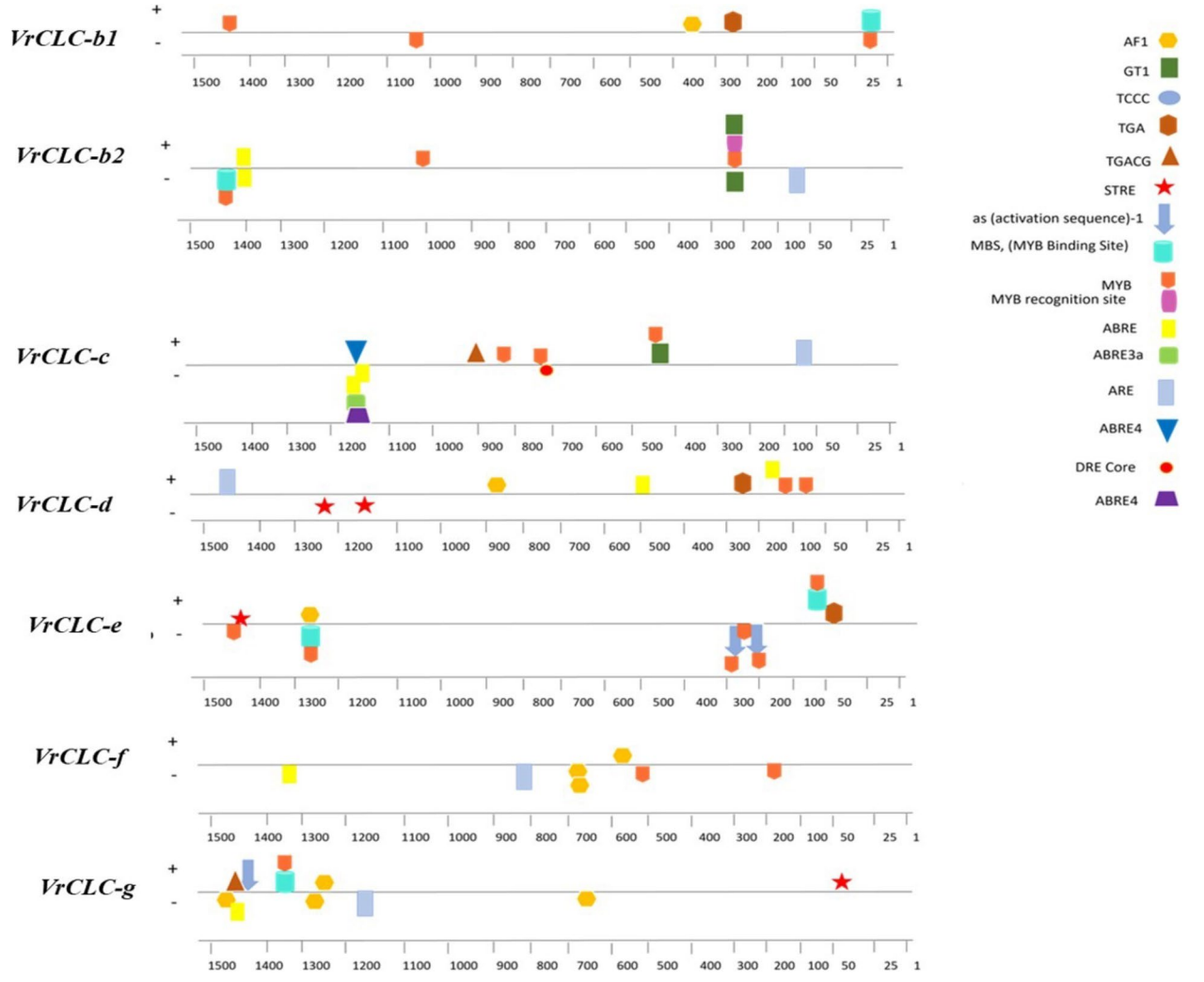

Fig. 5 Promoter Analysis. Promoter regions upstream of *VrCLC-b1*, *VrCLC-b2*, *VrCLC-c*, *VrCLC-d*, *VrCLC-e*, *VrCLC-f* and *VrCLC-g* (1500 bp) were analyzed for cis-regulatory elements. Various transcription factor binding sites and stress-responsive elements are highlighted with different symbols marked on the panel on right

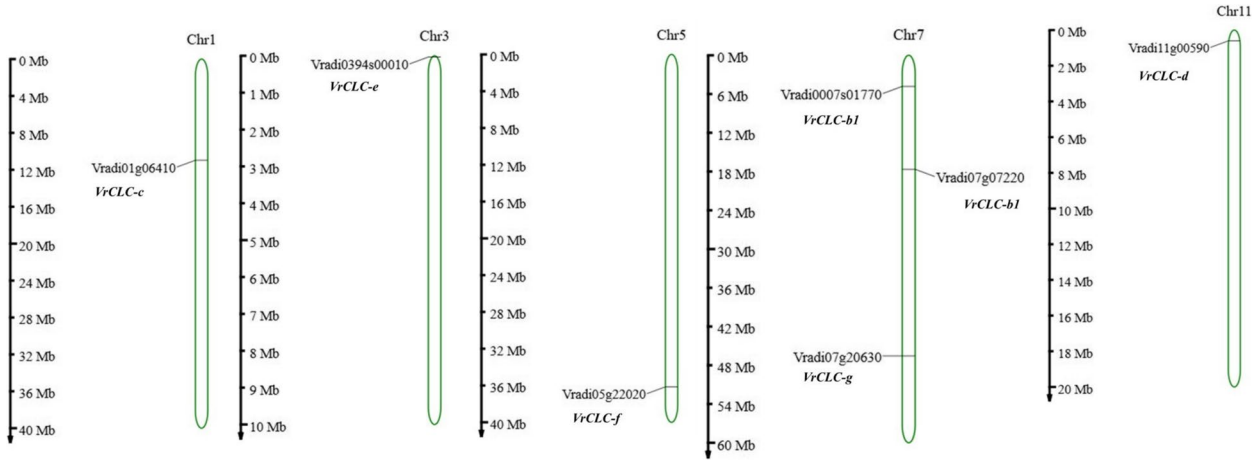

Fig. 6 The distribution of *CLC* genes on chromosomes of *V. radiata*. Chromosome numbers have been indicated on the top of each chromosome. The position of each gene on the respective chromosome has been depicted in terms of mega base-pairs of each gene. (MG2C_v2.1)

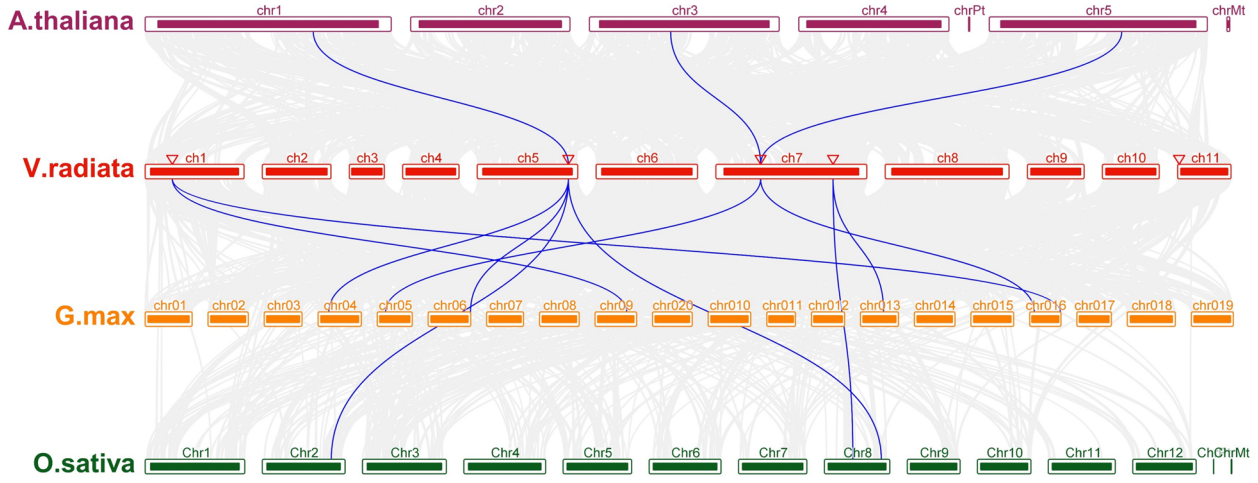

Fig. 7 Synteny analysis of *CLC* genes between *V. radiata* and representative plant species *i.e., A. thaliana, G. max* and *O. sativa*. Gray lines in the background indicate the collinear blocks within *Vigna radiata* and other plant genomes, while the blue lines highlight the syntenic *CLC* gene pairs

implying a regulatory role during abiotic stresses such as drought and salinity. STRE (stress response elements) were found in *VrCLC-d*, *VrCLC-e*, and *VrCLC-g*, further supporting their potential involvement in stress adaptation, whereas ARE (anaerobic responsive element) in *VrCLC-b2*, *VrCLC-c*, *VrCLC-d*, and *VrCLC-g*, suggests a possible role in gene expression under low-oxygen conditions. Other notable elements included the TGACG motif, associated with jasmonic acid response; DRE core elements, linked to drought stress response; GT1 elements for light responsiveness; and AS-I elements, known for enhancer binding activity. Detailed information on the cis-elements is provided in Supplementary Table S4.

Chromosomal distribution of *VrCLC* genes

The genomic distribution of the *VrCLC* gene family was analyzed and mapped onto the *V. radiata* chromosomes. The seven *VrCLC* genes were found to be unevenly distributed across six chromosomes. *VrCLC-b1*, *VrCLCb-2,* and *VrCLC-g* were located on chromosome 7 at three loci, *i.e., Vradi07g07220* at 17 Mb, *Vradi0007s01770* at 5.6 Mb and *Vradi07g20630* at 45 Mb respectively. *VrCLC-c* was located on chromosome 1 (*Vradi01g06410*, 11 Mb), *VrCLC-d* on chromosome 11 (*Vradi11g00590*, 0.5 Mb), *VrCLC-e* on chromosome 3, (Vradi0394s00010, scaffold_394) and *VrCLC-f* on chromosome 5, (*Vradi05g22020,* 37.1 Mb) and (Fig. 6).

Synteny and evolutionary analyses of mungbean genes and other plants CLCs

VrCLC genes were further examined through a comprehensive synteny analysis with three reference species *i.e. Arabidopsis thaliana, Glycine max*, and *Oryza sativa* which revealed multiple orthologous gene pairs, indicating conserved evolutionary relationships (Fig. 7).

Table 2 Predicted Ka/Ks ratio of the duplicated gene pairs: NaN-not a number (In the Ka or Ks values, if zero occurs then it shows NaN)

Duplicated gene pair		Ka	Ks	Ka/Ks
Gene 1	**Gene 2**			
Vradi01g06410.1	KRH09287	0.103487	0.245365	0.421768
Vradi01g06410.1	KRH38788	0.103627	0.267562	0.387303
Vradi05g22020.1	KRH62543	0.04949	0.194733	0.254141
Vradi05g22020.1	KRH56382	0.045594	0.215017	0.212047
Vradi05g22020.1	AT1G55620.2	0.20717	1.538307	0.134674
Vradi07g20630.1	KRH20184	0.395781	2.773392	0.142707
Vradi07g07220.1	AT3G27170.1	0.139222	1.982131	0.070239
Vradi07g07220.1	AT5G40890.1	0.146228	NaN	NaN
Vradi07g07220.1	KRH06955	0.083131	0.530414	0.156728
Vradi07g07220.1	KRH57669	0.028815	0.303767	0.09486
Vradi05g22020.1	Os02t0720200	0.966538	NaN	NaN
Vradi05g22020.1	Os08t0499200	0.225552	1.611344	0.139977
Vradi07g20630.1	Os08t0300300	0.94382	2.206148	0.427814

Ks, the number of synonymous substitutions per synonymous site; Ka, the number of non-synonymous substitutions per nonsynonymous site; NaN- not a number (if there is no ka or ks substitution or if zero accours then it shows NaN)

Several *VrCLC* genes located on chromosomes 1, 5, and 7 showed syntenic connections with *Arabidopsis* chromosomes 1, 3, and 5, and with corresponding regions in *G. max* and *O. sativa*. The two legumes *V.radiata* and *G.max* showed the highest number of syntenic links consistent with their close evolutionary relationship. Among the seven *VrCLC* genes, the Ka/Ks ratio values were calculated and observed to be less than one for all gene pairs, indicating that these genes are under purifying selection (Table 2).

WGCNA analysis

Using the RNA-seq data, WGCNA analysis was performed for *VrCLC* genes that revealed numerous potential interacting partners, suggesting their involvement in diverse cellular processes. A total of 220 genes were found to be co-expressed with five *VrCLC* genes (Fig. 8, Supplementary Fig, S1). Specifically, 60, 61, 14, 60 and 25 hub genes were co-expressed with *VrCLC-b1, VrCLC-b2, VrCLC-d, VrCLC-e* and *VrCLC-f* genes, respectively. The *VrCLC-b1* gene was co-expressed with defence-related genes, namely disease resistance protein (VRADI07G10190), MYB transcription factors (VRADI07G11510, VRADI07G29010) and HSP70 (VRADI07G21470). Similarly, the MYB transcription factor (VRADI0023S00060), zinc finger protein (VRADI0169S00070) and FAD-binding Berberine family protein (VRADI0048S00200) involved in plant metabolism and defense were co-expressed with *VrCLC-b2*. Furthermore, genes involved in plant growth, such as the sugar porter (SP) family MFS transporter (VRADI11G00610), lipid transfer protein (VRADI11G00870), auxin efflux carrier family protein (VRADI11G07270) and a pathogenesis-related thaumatin superfamily protein (VRADI11G02300) were co-expressed with *VrCLC-d*.

Similarly, *VrCLC-e* gene was co-expressed with a set of genes including the WRKY transcription factor (VRADI04G07130), cytochrome P450 superfamily protein (VRADI03G01370), disease resistance-responsive (VRADI04G10160), HSP70 (VRADI04G10800) and leucine-rich repeat receptor-like kinase (VRADI05G03950). Additionally, two transcriptional factors,

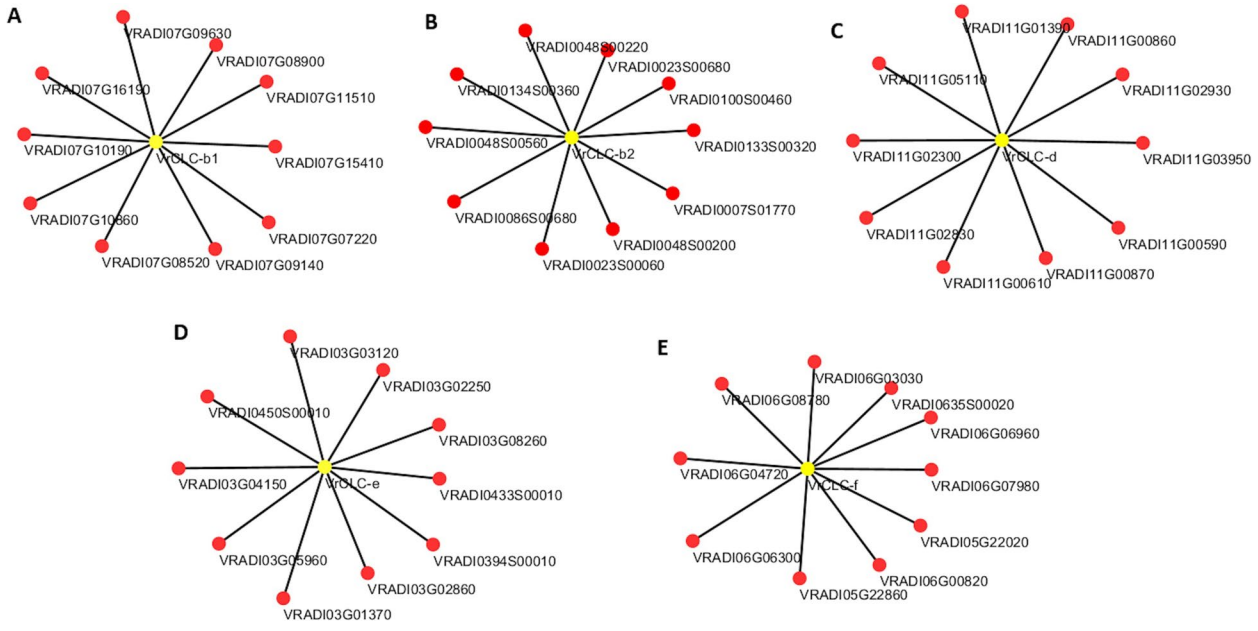

Fig. 8 WGCNA analysis. Weighted gene co-expression network analysis (WGCNA) of *VrCLC* genes.1–5: the co-expressed genes in the network of (1) *VrCLC-b1*, (2) *VrCLC-b2*, (3) *VrCLC-d* (4) *VrCLC-e* and (D) *VrCLC-f*. The VrCLC genes are marked in red

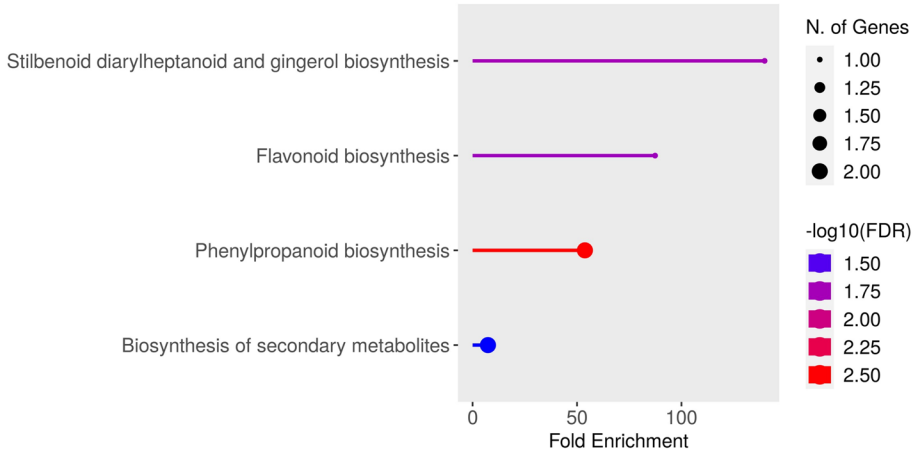

Fig. 9 Co-Expressed KEGG analysis. KEGG pathway enrichment analysis of differentially expressed genes. The x-axis indicates the fold enrichment of genes associated with each pathway. Dot size represents the number of genes involved, while color intensity corresponds to the statistical significance measured by $-\log_{10}$(FDR). Pathways such as Stilbenoid, diarylheptanoid and gingerol biosynthesis, Flavonoid biosynthesis, and Phenylpropanoid biosynthesis showed significant enrichment. The background color gradient corresponds to the corrected false discovery rate (FDR), with red indicating higher statistical significance

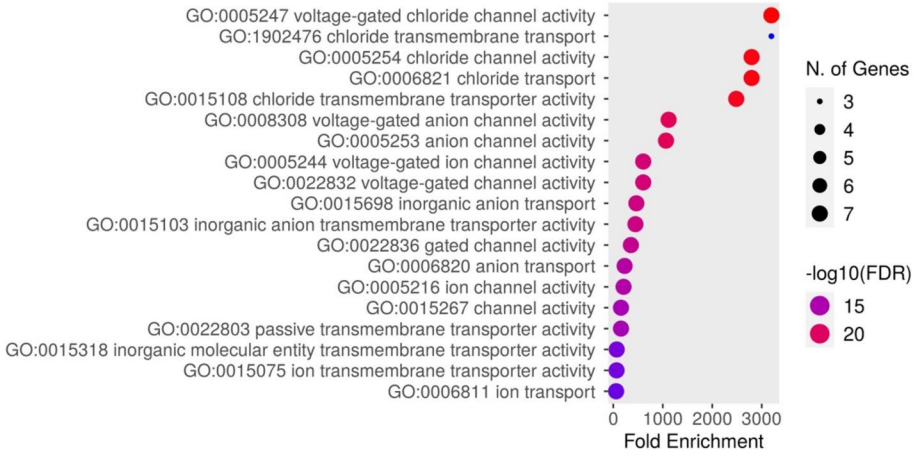

Fig. 10 Co-Expressed GO analysis. Gene Ontology (GO) enrichment of genes related to ion and chloride transport. The x-axis shows fold enrichment for each GO term. Dot size represents the number of associated genes, and color indicates statistical significance ($-\log_{10}$FDR). The enriched terms include voltage-gated chloride channel activity (GO:0005247), chloride transmembrane transport (GO:1,902,476), and chloride channel activity (GO:0005254), highlighting the importance of ion transport processes under the studied conditions

WRKY40 (VRADI06G13510) and C2-H2 zinc finger protein (VRADI06G13990) along with RING/FYVE/PHD zinc finger superfamily protein (VRADI06G08780) and scarecrow-like protein 32 (VRADI05G22860) belonging to the GRAS transcription factor were co-expressed with *VrCLC-f* gene. KEGG pathway analysis categorized these hub genes into several pathways, including phenylpropanoid biosynthesis, pentose and glucuronate interconversions, metabolic pathways, biosynthesis of secondary metabolites, glucosinolate biosynthesis, etc., (Fig. 9, Supplementary Table S6, and S7). However, a majority of the hub genes were not annotated in KEGG pathways. Similarly, Gene ontology (GO) analysis was performed categorizing most of the genes into voltage-gated chloride channel activity, chloride channel activity, chloride transmembrane transport, chloride transport etc. (Fig. 10; Supplementary Table S5).

Protein modelling for VrCLC proteins

The 3D structural models of VrCLC proteins (A–G) revealed that all proteins adopt a typical CLC protein fold comprising multiple α-helices spanning the membrane and short β-strands (Fig. 11). Their structure is composed of α-helixes, β-sheets, and coiled-coil (Fig. 11). The spatial arrangement of helices and loops varied slightly among the proteins, indicating possible structural divergence associated with their functional specialization. Seven VrCLC proteins consist of the following secondary structures: 26–31 α-helixes, 7–9 β-sheets, and 33–37 coiled-coils (Supplementary Table S8). The TM

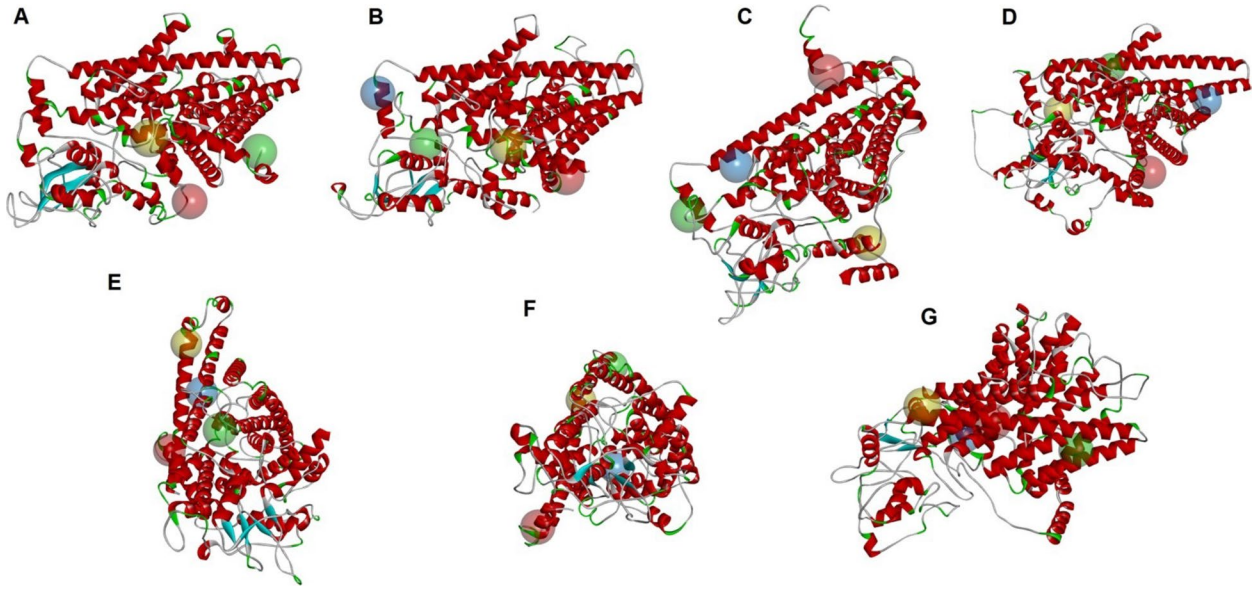

Fig. 11 Protein modelling for VrCLC genes. Predicted three-dimensional homology structure of greengram VrCLC proteins. The final 3D structures of VrCLC proteins were built by Discovery Studio v.21.1. The secondary structural components: α-helices (red), β-sheets (cyan), coils (green), and loops (gray) as well as the top four putative-binding sites: site 1 (yellow sphere), site 2 (green sphere), site 3 (red sphere), and site 4 (blue sphere) are indicated in the predicted 3D models of **A**. VrCLC-b1; **B**. VrCLC-b2; **C**. VrCLC-c; **D**. VrCLC-d; **E**. VrCLC-e; **F**. VrCLC-f and **G**. VrCLC-g

scores and RMSD values of the predicted models ranged from 0.47 to 0.62 and 9.9 to 11.4, respectively. Similarly, c-scores, number of decoys, and cluster density values were calculated to assess confidence and quality of the conserved protein models. Additionally, potential ligand-binding sites were also predicted to provide insights into possible interactions with diverse molecules (Supplementary Table S9).

Chloride ion estimation

Plant material from mungbean was used to estimate chloride (Cl^-) accumulation in roots, leaves, stems, flowers, IMC, RN, and seeds. Chloride content was measured under two NaCl treatments: control (untreated), 100 mM NaCl, and 200 mM NaCl. Leaves and stems showed the highest chloride accumulation, followed by flowers and IMC, whereas roots and RN had comparatively lower levels, and seeds exhibited the least chloride content. In roots, Cl^- content increased significantly from 0.9% in control to approximately 1.7% under 100 mM NaCl and 1.9% under 200 mM NaCl treatment. In leaves, Cl^- content increased from 1.1% (control) to 2.2% (100 mM) and 3.4% (200 mM) under salt treatment. In stems, Cl^- content was 2.4% in control plants, which showed a significant increase to 3.2% at 200 mM. Similarly, flowers also showed an increase in Cl^- content to 2.2% at 200 mM NaCl stress as compared to 1.4% in control plants. In IMC samples, Cl^- content increased from 1.2% in control to 2.2% and 2.4% at 100 and 200 mM NaCl respectively. Root nodules showed relatively smaller insignificant changes. Finally, in seeds, Cl^- content remained consistent across treatments, with all three groups (control, 100 mM, and 200 mM) showing 0.6% Cl^-, representing the lowest accumulation among all tissues analysed (Fig. 12).

Heatmap for expression of *VrCLC* gene under salinity stress

Expression profiling of *VrCLC* genes was done in plants 45 days after salt treatment that showed distinct tissue-specific and concentration-dependent expression patterns (Fig. 13). In the heatmap, lower expression levels are represented by deep purple/blue, while higher expression levels are shown in bright yellow/light green. At 100 mM NaCl, *VrCLC-b1* displayed the highest expression in roots and leaves, while *VrCLC-g* was strongly upregulated in flowers. *VrCLC-b2, VrCLC-d,* and *VrCLC-e* exhibited moderate expression across vegetative tissues, whereas *VrCLC-c* and *VrCLC-f* showed comparatively lower expression. At 200 mM NaCl, *VrCLC-e, VrCLC-g,* and *VrCLC-b1* were markedly upregulated in various tissues, suggesting their potential roles in chloride transport under severe salt stress. These results indicate functional diversification of *VrCLC* genes in mediating tissue-specific responses to salinity.

Time-course expression profiling of different *VrCLC* genes in leaf and root tissues under NaCl stress

Time-course expression analysis of *VrCLC* genes under salt stress showed distinct temporal regulation patterns in leaves and roots (Fig. 14). In leaves, *VrCLC-b1* exhibited an initial downregulation up to 24 h, followed by significant upregulation at 72 h and beyond under salt stress.

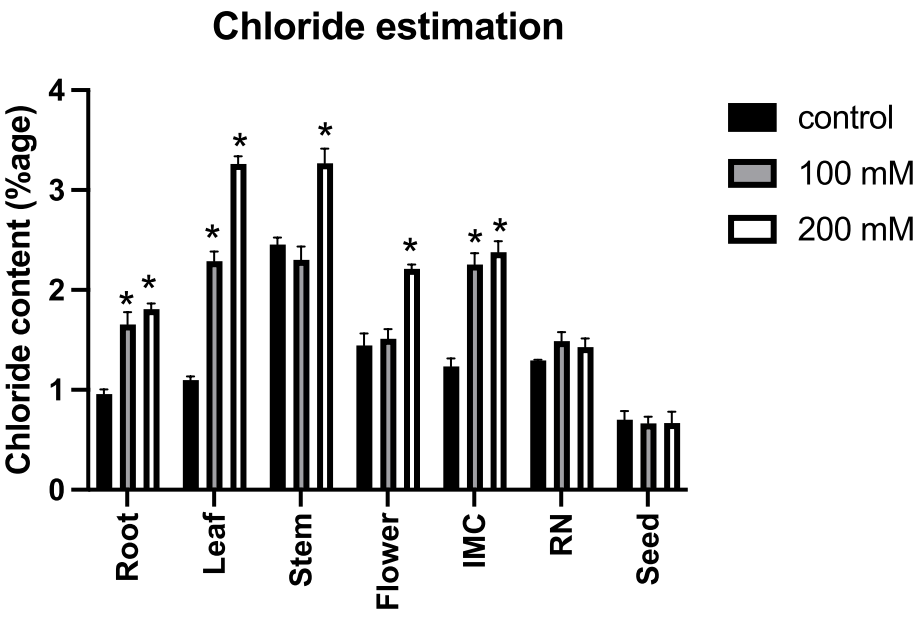

Fig. 12 Chloride estimation of greengram tissues with two NaCl treatment Chloride content (% dry weight) was quantified in root, leaf, stem, flower, immature cotyledon (IMC), root nodule (RN), and seed tissues of plants subjected to control (black bars), 100 mM NaCl (gray bars), and 200 mM NaCl (white bars) treatments. Data represent mean ± SE of three biological replicates. *- indicate statistically significant differences ($p < 0.05$) compared to control

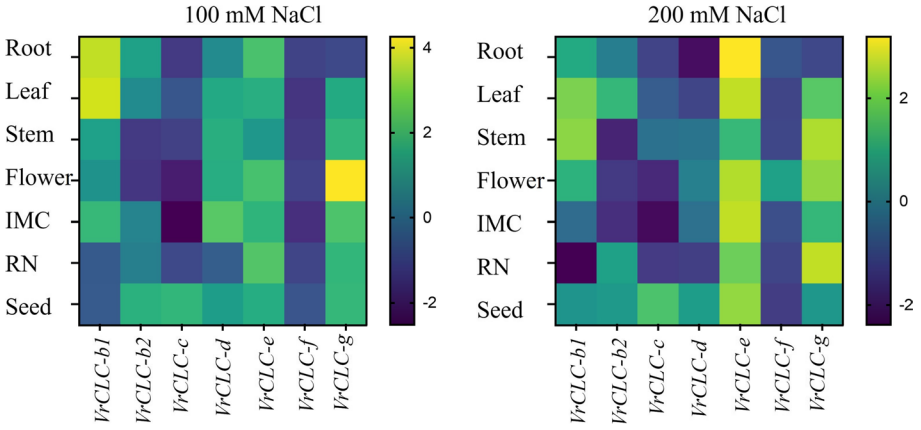

Fig. 13 Heatmap visualization of expression of *CLC* genes with different tissue samples Heatmaps showing the relative expression levels (log_2 fold change) of seven *VrCLC* genes in various tissues (Root, Leaf, Stem, Flower, IMC – immature cotyledon, RN – root nodule, Seed) of mungbean under (A) 100 mM NaCl and (B) 200 mM NaCl treatments. Color scale represents expression values, with yellow indicating higher expression and purple indicating lower expression relative to control conditions

A similar pattern was observed in root tissues, where a significant down-regulation was observed till 72 h NaCl treatment and the upregulation was observed only at day 10 in 200 mM NaCl. In leaf, *VrCLC-b2* was strongly upregulated after 7 d while in roots, it showed a distinct concentration dependent regulation where the expression was upregulated only at 200 mM NaCl. *VrCLC-c* showed consistent downregulation till 7 days post salt treatment in leaf and root, with *VrCLC-d* displaying late upregulation after 7–10 d in leaf and after 72 h in root tissue. These patterns suggest that *VrCLC-b1*, *VrCLC-b2*, and *VrCLC-d* are inducible under prolonged salt stress, while *VrCLC-c* is negatively regulated, indicating differential roles of these genes in salinity response.

VrCLC-e showed strong and early induction in leaves under 200 mM NaCl, with significant upregulation persisting up to 7 days, whereas in roots, its expression gradually increased after 24 h (Fig. 15). *VrCLC-f* was consistently downregulated in leaves at almost all time points, while in roots, it displayed transient upregulation at 6 h, followed by repression at later stages (Fig. 15). *VrCLC-g* exhibited significant induction in leaves under 200 mM NaCl at multiple time points, while in roots it showed transient upregulation at 24 h but remained downregulated at other time points (Fig. 15).

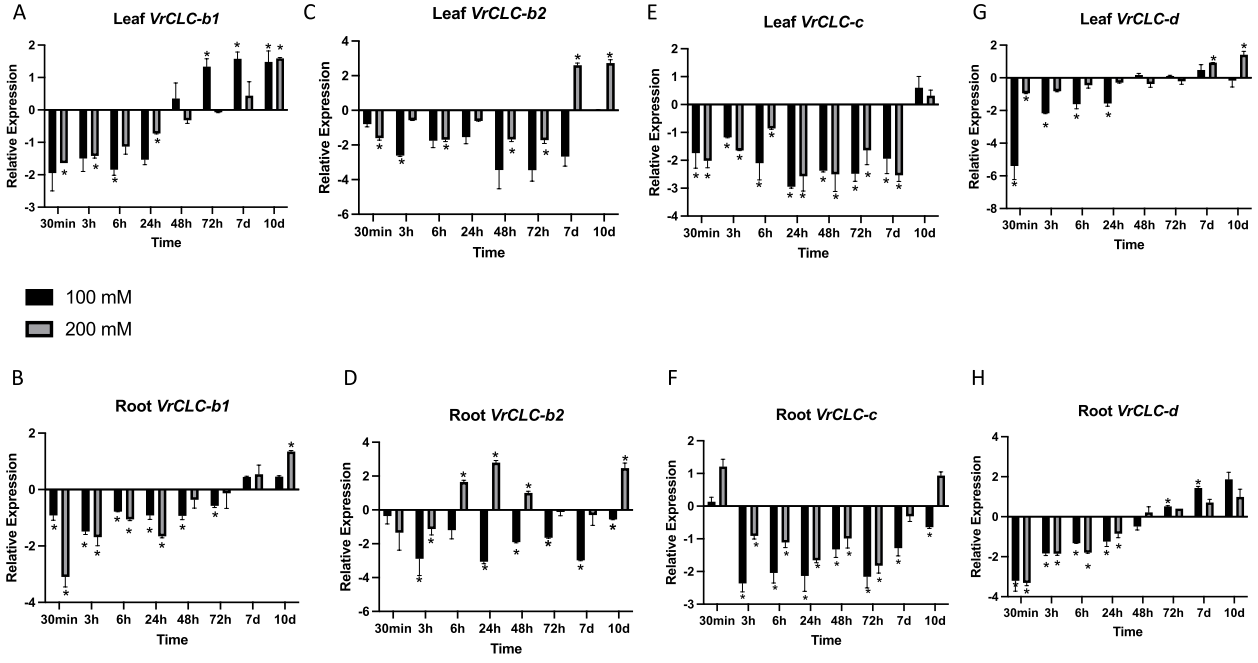

Fig. 14 Expression profiles of *VrCLC* genes. Relative expression (log_2 fold change) of *VrCLC* genes in leaves and roots of mungbean plants treated with 100 mM and 200 mM NaCl. Panels show expression of *VrCLCb1* (**A**, **B**), *VrCLCb2* (**C**, **D**), *VrCLCc* (**E**, **F**), and *VrCLCd* (**G**, **H**). Bars represent mean ± SD of three biological replicates, each based on three technical replicates

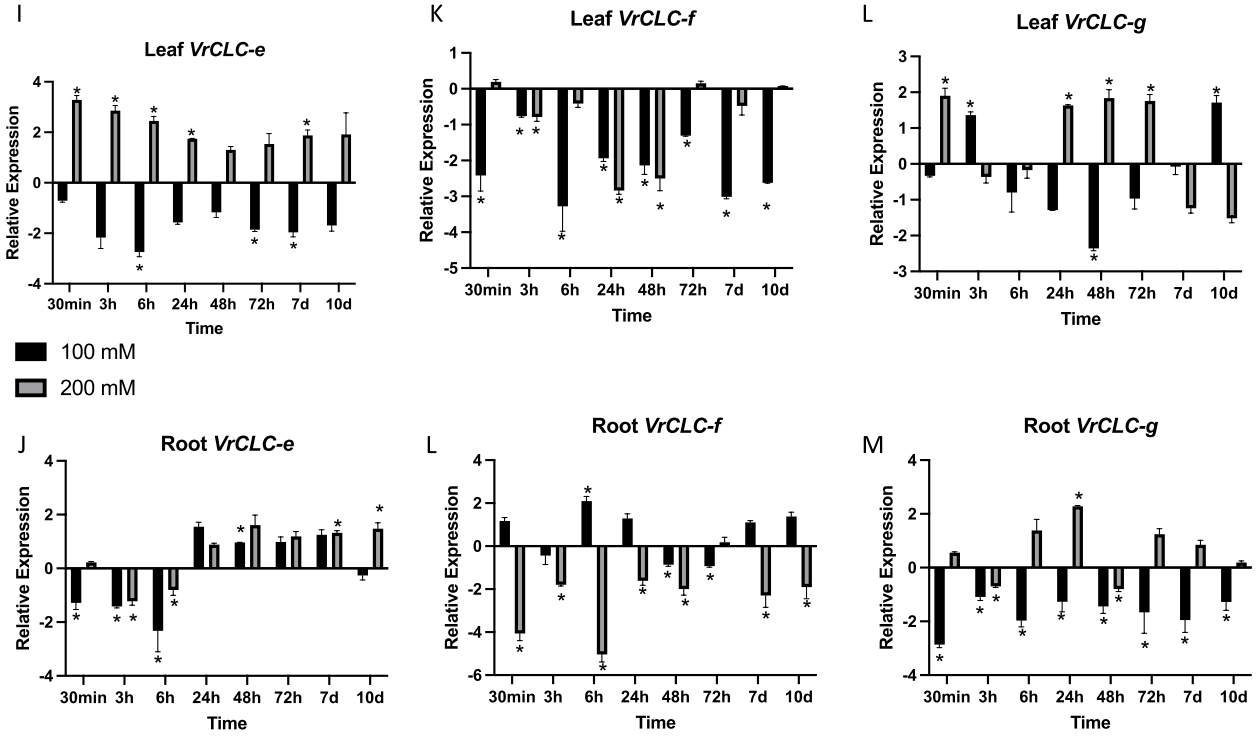

Fig. 15 Expression profiles of *VrCLC* genes. Relative expression (log_2 fold change) of *VrCLC* genes in leaves and roots of mungbean plants treated with 100 mM and 200 mM NaCl. Panels show expression of *VrCLCe* (**I**, **J**), *VrCLCf* (**K**, **L**), and *VrCLCg* (**M**, **N**). Bars represent mean ± SD of three biological replicates, each based on three technical replicates

These results indicate that *VrCLC-e* and *VrCLC-g* are predominantly salt-inducible in leaves, whereas *VrCLC-f* is largely repressed, suggesting functional divergence of these genes in salt stress adaptation.

Discussion

CLCs are a well-characterized family of anion transporters for Cl^-, NO_3^-, and SO_4^{2-} that play essential roles in nutrient uptake and transport, regulation of cellular turgor, stomatal movement, and signal transduction [19, 45]. They are also actively implicated in plant salt tolerance [3]. Genome-wide identification and functional characterization of *CLC* gene families have been reported in several plant species, including *Arabidopsis* [46], wheat [25], cotton [47], pomegranate [48], trifoliate orange [49], *Nicotiana* [13], and tomato [50] etc. However, such systematic studies remain limited to only a few crops, and no comprehensive analysis is currently available for mungbean. This knowledge gap prompted the present work, wherein we performed a comprehensive genome-wide identification, structural and evolutionary characterization, and expression profiling of the *CLC* gene family in mungbean, with particular emphasis on their potential roles in salinity stress responses.

We identified seven *VrCLC* genes in mungbean which is consistent with the modest size of the *CLC* gene family observed in many diploid plant species like *Arabidopsis* [50], pomegranate [48] and tomato [50] etc. Allopolyploid cotton has 22 *CLC* genes [47], and hexaploid wheat contains 23 *TaCLC* genes grouped into multiple homoeologous subfamilies [25]. The occurrence of multiple *CLC-b* and *CLC-d* paralogs in wheat and cotton is ascribed to genome duplications [25, 47]. In contrast, the smaller diploid genome of mungbean contains only a single copy for most clades except *VrCLC-b1/b2* that is the sole duplicate pair identified. This suggests that mungbean retains a core set of *CLC* genes that are functionally sufficient for carrying out anion homeostasis and may have evolved under stronger purifying selection for maintenance of critical function.

The gene structures of *VrCLCs* show variability in exon number ranging from 6 (*VrCLC-b1, -b2,—g*) to up to 24 exons (*VrCLC-d*). This resembles the variability observed in other plants like *Nicotiana* [13]. Such complex gene structures, could be a conserved phenomenon and potentially related to regulatory or splicing control mechanisms. Structural motifs identified in the in VrCLCs are rich in acidic (E, D) and basic (K, R) residues, which are characteristic of ion-binding and gating regions in known CLC antiporters [50]. Moreover, motifs 3, 5, and 7 contained key glutamate residues which are important determinants of Cl^-/H^+ antiport activity [51]. Additionally, predicted 3D models showcase classic features of CLC architecture such as predominant α-helical transmembrane domains forming ion conduction pores, presence of predicted ligand-binding pockets and at least one CLC-related domain (PF00654 or CBS-pair) in all gene, establishing their identity as functional CLC family members [52, 53]. Based on conserved glutamate-containing motifs (motifs 3, 5 and 7), domain organization, and phylogenetic relationship with *Arabidopsis* [46, 54], *VrCLC-b1, VrCLC-b2,* and *VrCLC-d* are predicted to function as Cl^-/H^+ antiporters. In contrast, *VrCLC-c, VrCLC-e, VrCLC-f,* and *VrCLC-g* likely function as chloride channels, lacking key proton-coupling glutamates and grouping with channel-type *Arabidopsis* homologs.

Phylogenetic analysis revealed that each mungbean CLC protein clustered with an orthologous clade in other species, though mungbean lacked a CLC-a clade member, unlike other legume crop soybean [13], suggesting a possible gene loss or divergence in its lineage. Comparative synteny between mungbean and soybean further clarifies *VrCLC* evolution (Fig. 7). The *Glycine max* genome is palaeopolyploid and experienced two whole-genome duplications (~59 and ~13 million years ago). This event left a high proportion of duplicated genes, whereas mungbean lacks the recent glycine-specific event and retains a more compact gene set [55, 56].Consistent with this history, soybean harbours a duplicated *CLC* repertoire (e.g., duplicated pairs such as *GmCLCb1/b2, GmCLCc1/c2, GmCLCd1/d2*), several of which are supported by functional or expression evidence under salinity [17, 23]. Our collinearity analysis shows that *VrCLC* loci on chromosomes 1, 5 and 7 correspond to duplicated *GmCLC* blocks on chromosomes 4, 5, 6, 9, 13 and 16, consistent with segmental retention following soybean whole-genome duplications, whereas mungbean largely maintains single-copy *VrCLC* loci. This difference in duplication history likely underpins the contrasting family sizes and paralog retention patterns between mungbean and soybean.

Promoter analysis of *VrCLC* genes revealed multiple hormone and stress-responsive cis-elements, including elements like TGA and AF1 that are associated with auxin signaling, indicating potential cross-talk with developmental and stress pathways. Reports from other species, such as *PtrCLC2* and *PtrCLC4* in trifoliate orange [49], and *CLC* genes in cotton [47] and soybean [57] shows that *CLC* transcripts are induced by NaCl and ABA, highlighting their integration into broader stress-responsive regulatory networks and a likely co-activation with other defense-related genes under adverse environmental conditions. WGCNA complements this notion, as *VrCLC-b1, b2, d, e,* and *f* were co-expressed with WRKYs, HSP70, and genes linked to metabolism and transport, connecting VrCLCs to defense and secondary metabolism pathways. Moreover, transcriptional regulators like GmbHLH3 [23] and GmZAT10-1 [58],

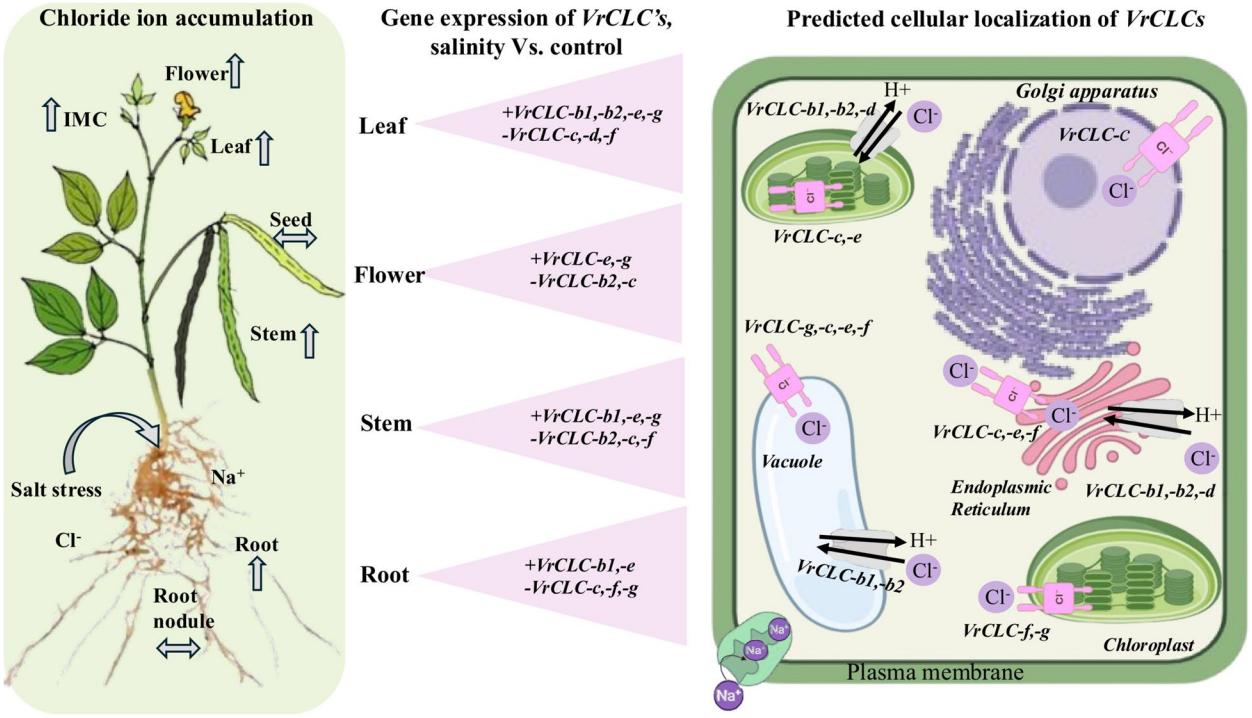

Fig. 16 Proposed model of *VrCLC* gene expression and localization in mung bean under salt stress. Schematic representation of chloride ion (Cl^-) accumulation in different tissues of mung bean under salt stress and the associated changes in *VrCLC* gene expression compared to control conditions (middle panel). Upregulated genes are indicated with a "+" sign, and downregulated genes with a "–" sign for each tissue type (Leaf, Flower, Stem, Root). The right panel shows the predicted subcellular localization of *VrCLC* proteins, including the vacuole, chloroplast, Golgi apparatus, endoplasmic reticulum, and plasma membrane, with proposed roles in Cl^- transport and exchange with protons (H^+). Na^+ distribution under salt stress is also represented

previously implicated in salt stress responses in soybean, represent potential candidates that may regulate *VrCLC* expression in mungbean, although this requires further experimental confirmation.

In our previous work comparing three mungbean varieties differing in salt tolerance, we demonstrated that selective exclusion of Cl^- ions, accompanied by reduced expression of *CLC* genes, *VrCLC-b2* and *VrCLC-c* in leaf tissue contributed to the enhanced salinity tolerance of the salt resistant variety MGG 295, despite substantial Na^+ accumulation in leaves [3]. In contrast, the salt-sensitive line LGG 460 showed higher Cl^- uptake along with markedly increased expression of *VrClC-b2* and *VrClC-c* in both roots and shoots, highlighting that excessive Cl^- accumulation likely contributes to salt-induced toxicity symptoms. In this study also, we performed the quantification of Cl^- ion accumulation in different tissues of the plant under salt stress. It was interesting to observe that Cl^- content increased in leaf, IMC and roots at both the NaCl concentrations, while stem and flower accumulated Cl^- only at 200 mM NaCl. Expression heatmaps obtained from qRT-PCR analysis of *CLC* genes revealed strong induction of *VrCLC-b1* and *e* in leaf and roots under 100 mM and 200 mM NaCl, coinciding with elevated Cl^- content in these tissues, *VrCLC-b1* particularly showed no change or rather downregulation in root nodules and seed where we observe no change in Cl^- accumulation. This correspondence suggests that *VrCLC-b1* may contribute to Cl^- transport from roots to leaves and IMC while its unchanged or lower expression prevented excessive Cl^- translocation to root nodules and seeds. Similarly, the Cl^- accumulation only at 200 mM NaCl in stem and flower could potentially be mediated by induced expression of *VrCLC-b1, -e* and *-g*. In contrast, genes such as *VrCLC-c* and *VrCLC-f* displayed weaker induction, indicating their minor contribution to Cl^- redistribution. Together, these patterns indicate that differential activation of *VrCLC* members under salt stress may underpin the observed ionic balance and tissue-specific Cl^- compartmentation in mungbean. Time-course qRT-PCR expression analysis in root and leaf samples indicated that *VrCLC-b1, -b2,* and *-d* were initially downregulated but strongly induced at later stages, suggesting roles in long-term Cl^- sequestration. *VrCLC-e*'s early and sustained induction, could imply rapid stress sensing, whereas *VrCLC-g* showed robust but transient induction in leaves, and *VrCLC-f* was consistently repressed (Fig. 16). Early salt exposure often triggers osmotic adjustment and signaling (e.g., ROS, ABA, calcium), while suppressing energy-intensive processes like ion transport/sequestration. This is consistent with the biphasic expression patterns reported for other stress-responsive

genes in *Arabidopsis,* where an initial suppression phase is followed by later transcriptional activation [59]. Notably, our previous findings showed that MGG 295 limits Cl^- accumulation under salinity stress (80 and 160 mM NaCl), accompanied by downregulation of *VrCLC-b2* and -c [3]. Here, also a similar down-regulation of expression was observed initially till 72 h and thereafter we observed upregulation in *VrCLC-b1/b2* particularly at 200 mM, indicating that these genes are activated primarily under more severe stress conditions. This is in contrast to sensitive mungbean and *Arabidopsis* genotypes [3, 47], where early and robust induction of CLC genes typically forms part of the acclimation response. These findings highlight distinct temporal and stress-intensity dependent regulatory strategies governing chloride homeostasis under salt stress. Taken together, our genome-wide analysis provides a foundational framework for understanding the structural and functional diversity of *VrCLC* genes in mungbean. The strong salt-responsive expression of *VrCLCb1/b2*, *VrCLCe*, and *VrCLCg*, together with their association with Cl^- distribution, identifies these genes as promising candidates for improving ion balance and adaptation under salinity stress. From an applied perspective, these *VrCLC* members could serve as molecular markers in marker-assisted breeding programs or as functional targets for CRISPR/Cas-based genome editing to develop salt-tolerant mungbean cultivars.

Conclusion

This study provides the first comprehensive characterization of the *VrCLC* gene family in mungbean, revealing seven members with diverse gene structures, conserved motifs, and phylogenetic relationships consistent with other dicot and monocot species. The strong synteny with *Glycine max* and *Arabidopsis* highlight their evolutionary conservation and functional importance in anion transport. The strong induction of *VrCLC-e* and *VrCLC-g* between 30 min to 24 h at 200 mM NaCl (~ 2- to fourfold increase) suggests their possible role as early responders to salt stress, functioning in initial Cl^- compartmentalisation or transport regulation (Fig. 16). On the other hand, the induction of *VrCLC-b1, b2,* and *d* (~ 2- to fourfold increase) from 72 h to 10 days under salt stress together with the chloride accumulation pattern, reveal that *VrCLC-b1/b2* and *-d* are potentially involved in long-term Cl^- sequestration. However, further functional validation is required to confirm this role. WGCNA and promoter analysis further suggest that these genes are integrated into broader stress-response networks and may influence not only ion homeostasis but also metabolic and defense pathways. Besides, low Cl^- levels in root nodules and reduced expression of most of the *VrCLC* genes, despite high salinity highlights a potential mechanism to safeguard nitrogen fixation from high Cl^- levels and could be promising targets for breeding salt-tolerant symbiotic performance (Fig. 16). Future work should focus on functional validation of key *VrCLC* genes, particularly *VrCLC-b1/b2*, *VrCLC-e*, and *VrCLC-g*, using CRISPR/Cas-mediated genome editing to elucidate their precise roles in Cl^- transport and salt tolerance. In parallel, promoter engineering or cis-element modulation could be employed to fine-tune *VrCLC* expression for achieving optimal ion balance under salinity. Besides, exploring natural allelic variation in *VrCLC* genes across *Vigna* germplasm and identifying key transcriptional regulator, could provide new avenues to enhance mungbean salinity tolerance. Such interventions may accelerate the development of salt-tolerant mungbean cultivars through precision breeding strategies.

Supplementary Information

The online version contains supplementary material available at https://doi.org/10.1186/s12864-025-12377-0.

Supplementary Material 1.

Acknowledgements
Not applicable.

Authors' contributions
A.T. conducted the experimental work, A.T., D.D. performed the *in silico* analysis and wrote the manuscript, P.B.K edited the manuscript, I.S. conceived and designed the study, analysed the data, wrote the manuscript. All authors reviewed the manuscript.

Funding
IS thanks Department of Biotechnology, Govt. of India for funding assistance in the form of Ramalingaswami Fellowship (Grant no. BT/RLF/Re-entry/48/2018). PBK is supported by the NASI-Platinum Jubilee Senior Scientist position.

Data availability
All datasets analysed in this study were obtained from publicly accessible repositories.
—**Genome and protein sequence data for** ***Vigna radiata*** were downloaded from the Ensembl plants database (https:/plants.ensembl e.org/Vigna_radiata/Info/Index) (accession IDs listed in supplementary table S1 as *Vradi07g07220* (*Vrclc-b1*), *Vradi0007s01770* (*Vrclc-b2*), *Vradi01g06410* (*Vrclc-c), Vradi11g00590* (*Vrclc-d), Vradi0394s00010* (*Vrclc-e), Vradi05g22020* (*Vrclc-f), Vradi07g20630 (Vrclc-g).*
—**Reference** ***CLC*** **gene sequences** were obtained from the publicly available databases for *Arabidopsis thaliana* (The Arabidopsis Information Resource Database, https:/www.arabidopsis.org/), *Oryza sativa* (Rice Genome Annotation Project Database, https:/rice.uga.edu/), *Glycine max* (LegumeMine, https:/mines.legumeinfo.org/), *Solanum lycopersicum* (Phytozome, https:/phytozome-next.jgi.doe.gov/), *Triticum aestivum* (Ensembl Plants https:/plants.ensembl.org/index.html), *Gossypium hirsutum* (Phytozome, https:/phytozome-next.jgi.doe.gov/). Accession numbers for all reference proteins are provided in Supplementary Table S2. These are as follows: *TaCLC-a-6AS-2 (TraesCS6A02G098600.1), TaCLC-b-6A (TraesCS6A02G098600.1), TaCLC-d-4D (TraesCS4A02G277600.2), TaCLC-d-4B (TraesCS4B02G035500), TaCLC-d-4A (TraesCS4A02G277600), TaCLC-g-1(TraesCS5A02G449500), TaCLC-g-2 (TraesCS5B02G457100), TaCLC-g-3 (TraesCS5D02G456000), TaCLC-a-6BS-1 (TraesCS6B02G126400.1), TaCLC-a-6DS-1 (TraesCS6D02G084300.1), TaCLC-a-6AS-1 (TraesCS6A02G098500.2), TaCLC-a-6DS-1 (TraesCS6D02G084300.1), TaCLC-c-3B (TraesCS3B02G144700), TaCLC-c-2A (TraesCS2A02G309900), TaCLC-c-2B (TraesCS2B02G326900), TaCLC-c-2D (TraesCS2D02G308100), TaCLC-b-6B (TraesCS6B02G126400), TaCLC-b-6D-1 (TraesCS6D02G084300, SlCLC-g (Solyc07g007690.4.1), SlCLC-f-1 (Solyc07g066210.3.1), SlCLC-a

(Solyc02g068080.3.1), SlCLC-c-1 (Solyc01g103140.3.1), SlCLC-f-2 (Solyc10g005690.3.1), GmCLC-a-1 (Glyma.05G077100), GmCLC-b1 (Glyma16g06190), GmCLC-d (Glyma11g00690), GmCLC-g-1 (Glyma13g23080), GmCLC-g-2 (Glyma13G161800), GmCLC-c-1 (Glyma16g33351), GmCLC-c-3 (Glyma16G208400), GmCLC-a-2 (Glyma.16g057600), GmCLC-b2 (Glyma19g25680), GmCLC-c-2 (Glyma.09G157900), GmCLC-f-1 (Glyma.04G114800), GmCLC-f-2 (Glyma.06G320900), GmCLC-e (Glyma.14G000500), GhCLC-c1 (Gohir.A10G115100), GhCLC-c3 (Gohir.A12G002100), GhCLC-c-2 (Gohir.A11G058300), GhCLC-c-4 (Gohir.D11G062600), GhCLC-g-2 (Gohir.A06G053000), GhCLC-g-4 (Gohir.D06G052000), GhCLC-g-1 (Gohir.A05G013900), GhCLC-g-3 (Gohir.D05G015000), GhCLC-a-1 (Gohir.A05G339200), GhCLC-a-2 (Gohir.A07G227500), GhCLC-a-4 (Gohir.D07G234600), GhCLC-f-2 (Gohir.A13G128000), GhCLC-f-4 (Gohir.D13G131500), GhCLC-f-1 (Gohir.A11G276100), GhCLC-f-3 (Gohir.D11G286500), OsCLC-a (LOC_Os12g25200.1) OsCLC-b2 (LOC_Os08g20570), OsCLC-g (LOC_Os08g20570), OsCLC-b1 (LOC_Os12g25200.1), OsCLC-c (LOC_Os02g35190), OsCLC-d (LOC_Os03g48940), OsCLC-e (LOC_Os01g50860), OsCLC-f-2 (Os02t0720200-01), OsCLC-f-3 (Os08t0499200-01), OsCLC-f-4 (Os08t0499200-01), AtCLC-a (AT5G40890.1), AtCLC-b1 (AT3G27170), AtCLC-g (AT5G33280), AtCLC-d (AT5G26240), AtCLC-c (AT5G49890), AtCLC-f (AT1G55620), AtCLC-e (AT4G35440).*

—The following **publicly accessible web-based tools** were used for domain, motif, structural, and regulatory analyses. Pfam (http:/pfam.xfam.org/), InterPro (https:/www.ebi.ac.uk/interpro/), NCBI Conserved Domain Database (NCBI-CDD) (https:/www.ncbi.nlm.nih.gov/cdd/), EXPASY (https:/web.expasy.org/compute_pi/), SMART (http:/smart.embl.de/), MEME Suite (https:/meme-suite.org/meme/tools/meme), GSDS2 (http:/gsds.cbi.pku.edu.cn), PlantCARE (http:/bioinformatics.psb.ugent.be/webtools/plantcare/html/), iTOL (https:/itol.embl.de/), Cytoscape (https:/cytoscape.org/), I-TASSER (https:/aideepmed.com/I-TASSER/)—**RNA-sequencing** data for mungbean samples were downloaded from the NCBI Sequence Read Archive (SRA)(https:/www.ncbi.nlm.nih.gov/sra) using the Galaxy web platform (https:/usegalaxy.org). Three biological replicate accessions (SRR20997626, SRR20997627, SRR20997628) for control samples and three replicate accessions (SRR20997623, SRR20997624, SRR20997625) for treated samples were used for co-expression analysis.

Declarations

Ethics approval and consent to participate
Not applicable.

Consent for publication
Not applicable.

Competing interests
The authors declare no competing interests.

Received: 14 September 2025 / Accepted: 24 November 2025
Published online: 09 December 2025

References
1. Shrivastava P, Kumar R. Soil salinity: A serious environmental issue and plant growth promoting bacteria as one of the tools for its alleviation. Saudi J Biol Sci. 2014;22(2):123.62. https://doi.org/10.1016/j.sjbs.2014.12.001.
2. Qadir M, Quillérou E, Nangia V, Murtaza G, Singh M, Thomas RJ, et al. Economics of salt-induced land degradation and restoration. Nat Resour Forum. 2014;38:282–95. https://doi.org/10.1111/1477-8947.12054.
3. Talakayala A, Jupally Y, Asinti S, Mekala GK, Kirti PB, Sharma I. Differences in the regulation of ion imbalance in response to high Na+ load hint at differential strategies for salt-tolerance in mungbean genotypes (*Vigna radiata L.*). Plant Growth Regul. 2025;105(1):89–109. https://doi.org/10.1007/s10725-024-01257-4.
4. Shaddam MO, Islam MR, Ditta A, Ismaan HN, Iqbal MA, Al-Ashkar I, et al. Genotypic divergences of important mungbean varieties in response to salt stress at germination and early seedling stage. Pol J Environ Stud. 2024;33(5):1–12. https://doi.org/10.15244/pjoes/183567.
5. Isemura T, Kaga A, Tabata S, Somta P, Srinives P, Shimizu T, et al. Construction of a genetic linkage map and genetic analysis of domestication related traits in mungbean (*Vigna radiata*). PLoS One. 2012;7(8):e41304. https://doi.org/10.1371/journal.pone.0041304.
6. HanumanthaRao B, Nair RM, Nayyar H. Salinity and high temperature tolerance in mungbean [*Vigna radiata* (L.) Wilczek] from a physiological perspective. Front Plant Sci. 2016;7:957–77. https://doi.org/10.3389/fpls.2016.00957.
7. Singh AK, Singh P, Kumar R. Physiological role of salicylic acid and potassium nitrate in mitigating salinity stress in mung bean (*Vigna radiata L.*). Legume Res-An Intl J. 2025;1:7. https://doi.org/10.18805/LR-5451.
8. Ahmad P, Jaleel CA, Salem MA, Nabi G, Sharma S. Roles of enzymatic and nonenzymatic antioxidants in plants during abiotic stress. Crit Rev Biotechnol. 2010;30(3):161–75. https://doi.org/10.3109/07388550903524243.
9. Shi H, Ishitani M, Kim C, Zhu JK. The *Arabidopsis thaliana* salt tolerance gene SOS1 encodes a putative Na+/H+ antiporter. Proc Natl Acad Sci U S A. 2000;97(12):6896–901. https://doi.org/10.1073/pnas.120170197.
10. Sunarpi X, Horie T, Motoda J, Kubo M, Yang H, Yoda K, et al. Enhanced salt tolerance mediated by AtHKT1 transporter-induced Na+ unloading from xylem vessels to xylem parenchyma cells. The Plant J. 2005;44(6):928–38. https://doi.org/10.1111/j.1365-313X.2005.02595.x.
11. White PJ, Broadley MR. Chloride in soils and its uptake and movement within the plant: a review. Ann Bot. 2001;88(6):967–88. https://doi.org/10.1006/anbo.2001.1540.
12. Barbier-Brygoo H, De Angeli A, Filleur S, Frachisse JM, Gambale F, Thomine S, et al. Anion channels/transporters in plants: from molecular bases to regulatory networks. Annu Rev Plant Biol. 2011;62(1):25–51. https://doi.org/10.1006/anbo.2001.1540.
13. Zhang H, Jin J, Jin L, Li Z, Xu G, Wang R, et al. Identification and analysis of the chloride channel gene family members in tobacco (*Nicotiana tabacum*). Gene. 2018;676:56–64. https://doi.org/10.1016/j.gene.2018.06.073.
14. Jentsch TJ. CLC chloride channels and transporters: from genes to protein structure, pathology and physiology. Crit Rev Biochem Mol Biol. 2008;43(1):3–36. https://doi.org/10.1080/10409230701829110.
15. Xing A, Ma Y, Wu Z, Nong S, Zhu J, Sun H, et al. Genome-wide identification and expression analysis of the CLC superfamily genes in tea plants (*Camellia sinensis*). Functional & Integrative Genomics. 2020;20(4):497–508. https://doi.org/10.1007/s10142-019-00725-9.
16. De Angeli A, Monachello D, Ephritikhine G, Frachisse JM, Thomine S, Gambale F, et al. The nitrate/proton antiporter AtCLCa mediates nitrate accumulation in plant vacuoles. Nature. 2006;442(7105):939–42. https://doi.org/10.1038/nature05013.
17. Li WY, Wong FL, Tsai SN, Phang TH, Shao G, Lam HM. Tonoplast-located GmCLC1 and GmNHX1 from soybean enhance NaCl tolerance in transgenic bright yellow (BY)-2 cells. Plant Cell Environ. 2006;29(6):1122–37. https://doi.org/10.1111/j.1365-3040.2005.01487.x.
18. Wege S, Gilliham M, Henderson SW. Chloride: not simply a 'cheap osmoticum', but a beneficial plant macronutrient. J Exp Bot. 2017;68(12):3057–69. https://doi.org/10.1093/jxb/erx050.
19. Wege S, Jossier M, Filleur S, Thomine S, Barbier-Brygoo H, Gambale F, et al. The proline 160 in the selectivity filter of the Arabidopsis NO3−/H+ exchanger AtCLCa is essential for nitrate accumulation in planta. Plant J. 2010;63(5):861–9. https://doi.org/10.1111/j.1365-313X.2010.04288.x.
20. Luo Q, Yu B, Liu Y. Differential sensitivity to chloride and sodium ions in seedlings of *Glycine max* and *G. soja* under NaCl stress. J Plant Physiol. 2005;162(9):1003–12. https://doi.org/10.1016/j.jplph.2004.11.008.
21. Teakle NL, Real D, Colmer TD. Growth and ion relations in response to combined salinity and waterlogging in the perennial forage legumes *Lotus corniculatus* and *Lotus tenuis*. Plant Soil. 2006;289(1):369–83. https://doi.org/10.1007/s11104-006-9146-8.
22. Teakle NL, Flowers TJ, Real D, Colmer TD. Lotus tenuis tolerates the interactive effects of salinity and waterlogging by 'excluding' Na+ and Cl− from the xylem. J Exp Bot. 2007;58(8):2169–80. https://doi.org/10.1093/jxb/erm102.
23. Wei P, Wang L, Liu A, Yu B, Lam HM. GmCLC1 confers enhanced salt tolerance through regulating chloride accumulation in soybean. Front Plant Sci. 2016;7:1082. https://doi.org/10.3389/fpls.2016.01082.
24. Wei P, Che B, Shen L, Cui Y, Wu S, Cheng C, et al. Identification and functional characterization of the chloride channel gene, GsCLC-c2 from wild soybean. BMC Plant Biol. 2019;19(1):1–15. https://doi.org/10.1186/s12870-019-1732-z.
25. Mao P, Run Y, Wang H, Han C, Zhang L, Zhan K. Genome-wide identification and functional characterization of the chloride channel TaCLC gene family in wheat (*Triticum aestivum* L.). Front Genet. 2022;13:846795. https://doi.org/10.3389/fgene.2022.846795.
26. Gasteiger E, Hoogland C, Gattiker A, Duvaud SE, Wilkins MR, Appel RD, Bairoch A. Protein identification and analysis tools on the ExPASy server. In The

Proteomics Protocols Handbook. Springer Protocols Handbooks. (ed. Walker, J. M.) 571–607 (Humana Press, 2005). https://doi.org/10.1385/1-59259-890-0:571.
27. Horton P, Park KJ, Obayashi T, Fujita N, Harada H, Adams-Collier CJ, et al. WoLF PSORT: protein localization predictor. Nucleic Acids Res. 2007;35:W585-587. https://doi.org/10.1093/nar/gkm259.
28. Tamura K, Stecher G, Kumar S. MEGA11: molecular evolutionary genetics analysis version 11. Mol Biol Evol. 2021;38(7):3022–7. https://doi.org/10.1093/molbev/msab120.
29. Letunic I, Bork P. Interactive tree of life (iTOL) v5: an online tool for phylogenetic tree display and annotation. Nucleic Acids Res. 2021;49(W1):W293–6. https://doi.org/10.1093/nar/gkab301.
30. Wang J, Chitsaz F, Derbyshire MK, Gonzales NR, Gwadz M, Lu S, et al. The conserved domain database in 2023. Nucleic Acids Res. 2023;51(D1):D384-388. https://doi.org/10.1093/nar/gkac1096.
31. Lescot M, Dehais P, Thijs G, Marchal K, Moreau Y, Van de Peer Y, et al. PlantCARE, a database of plant cis-acting regulatory elements and a portal to tools for in silico analysis of promoter sequences. Nucleic Acids Res. 2002;30(1):325–7. https://doi.org/10.1093/nar/30.1.325.
32. Chen C, Chen H, Zhang Y, Thomas HR, Frank MH, He Y. TBtools: an integrative toolkit developed for interactive analyses of big biological data. Mol Plant. 2020;13(8):1194–202. https://doi.org/10.1016/j.molp.2020.06.009.
33. Koch MA, Haubold B, Mitchell-Olds T. Comparative evolutionary analysis of chalcone synthase and alcohol dehydrogenase loci in *Arabidopsis*, *Arabis*, and related genera (Brassicaceae). Mol Biol Evol. 2000;17(10):1483–98. https://doi.org/10.1093/oxfordjournals.molbev.a026248.
34. Wang Y, Tang H, DeBarry JD, Tan X, Li J, Wang X, et al. MCScanX: a toolkit for detection and evolutionary analysis of gene synteny and collinearity. Nucleic Acids Res. 2012;40(7):e49. https://doi.org/10.1093/nar/gkr1293.
35. Chen C, Wu Y, Li J, Wang X, Zeng Z, Xu J, et al. TBtools-II: a "one for all, all for one" bioinformatics platform for biological big- data mining. Mol Plant. 2023;16(11):1733–42. https://doi.org/10.1016/j.molp.2023.09.010.
36. Vandel J, Gheeraert C, Staels B, Eeckhoute J, Lefebvre P, Dubois-Chevalier J. GIANT: galaxy-based tool for interactive analysis of transcriptomic data. Sci Rep. 2020;10(1):19835. https://doi.org/10.1038/s41598-020-76769-w.
37. Andrews S. FastQC: a quality control tool for high throughput sequence data. 2010. https://www.bioinformatics.babraham.ac.uk/projects/fastqc.
38. Kim D, Paggi JM, Park C, Bennett C, Salzberg SL. Graph-based genome alignment and genotyping with HISAT2 and HISAT-genotype. Nat Biotechnol. 2019;37(8):907–15. https://doi.org/10.1038/s41587-019-0201-4.
39. Liao Y, Smyth GK, Shi W. Featurecounts: an efficient general-purpose program for assigning sequence reads to genomic features. Bioinforma. 2014;30(7):923–30. https://doi.org/10.1093/bioinformatics/btt656.
40. Love MI, Huber W, Anders S. Moderated estimation of fold change and dispersion for RNA-seq data with DESeq2. Genome Biol. 2014;15(12):550. https://doi.org/10.1186/s13059-014-0550-8.
41. Langfelder P, Horvath S. WGCNA: an R package for weighted correlation network analysis. BMC Bioinformatics. 2008;9(1):559. https://doi.org/10.1186/1471-2105-9-559.
42. Yang J, Yan R, Roy A, Xu D, Poisson J, Zhang Y. The I-TASSER suite: protein structure and function prediction. Nat Methods. 2015;12(1):7–8. https://doi.org/10.1038/nmeth.3213.
43. Xu D, Zhang Y. Improving the physical realism and structural accuracy of protein models by a two-step atomic-level energy minimization. Biophys J. 2011;101(10):2525–34. https://doi.org/10.1016/j.bpj.2011.10.024.
44. Skoog DA, West DM, Holler FJ, Crouch SR. Fundamentals of analytical chemistry. Fort Worth: Saunders College Pub.; 1996.
45. Rajappa S, Krishnamurthy P, Huang H, Yu D, Friml J, Xu J, et al. The translocation of a chloride channel from the Golgi to the plasma membrane helps plants adapt to salt stress. Nat Commun. 2024;15(1):3978. https://doi.org/10.1038/s41467-024-48234-z.
46. Lv QD, Tang RJ, Liu H, Gao XS, Li YZ, Zheng HQ, et al. Cloning and molecular analyses of the Arabidopsis thaliana chloride channel gene family. Plant Sci. 2009;176(5):650–61. https://doi.org/10.1016/j.plantsci.2009.02.006.
47. Liu X, Pi B, Pu J, Cheng C, Fang J, Yu B. Genome-wide analysis of chloride channel-encoding gene family members and identification of CLC genes that respond to Cl−/salt stress in upland cotton. Mol Biol Rep. 2020;47(12):9361–71. https://doi.org/10.1007/s11033-020-06023-z.
48. Liu C, Zhao Y, Zhao X, Dong J, Yuan Z. Genome-wide identification and expression analysis of the CLC gene family in pomegranate (*Punica granatum*) reveals its roles in salt resistance. BMC Plant Biol. 2020;20(1):560. https://doi.org/10.1186/s12870-020-02771-z.
49. Wei QJ, Gu QQ, Wang NN, Yang CQ, Peng SA. Molecular cloning and characterization of the chloride channel gene family in trifoliate orange. Biol Plant. 2015;59(4):645–53. https://doi.org/10.1007/s10535-015-0532-z.
50. Lv R, Mo F, Li C, Meng F, Zhang H, Yu L, et al. Genome-wide identification of the CLC gene family in tomato (*Solanum lycopersicum*) and functional analysis of SlCLC8 in salt stress tolerance. Sci Hortic. 2024;338:113754. https://doi.org/10.1016/j.scienta.2024.113754.
51. Bennetts B, Parker MW. Molecular determinants of common gating of a ClC chloride channel. Nat Commun. 2013;4(1):2507. https://doi.org/10.1038/ncomms3507.
52. Park K, Lee BC, Lim HH. Mutation of external glutamate residue reveals a new intermediate transport state and anion binding site in a CLC Cl−/H+ antiporter. Proc Natl Acad Sci U S A. 2019;116(35):17345–54. https://doi.org/10.1073/pnas.1901822116.
53. Estévez R, Pusch M, Ferrer-Costa C, Orozco M, Jentsch TJ. Functional and structural conservation of CBS domains from CLC chloride channels. J Physiol. 2003;557(2):363–78. https://doi.org/10.1113/jphysiol.2003.058453.
54. Wang K, Preisler SS, Zhang L, Cui Y, Missel JW, Grønberg C, et al. Structure of the human ClC-1 chloride channel. PLoS Biol. 2019;17(4):e3000218. https://doi.org/10.1371/journal.pbio.3000218.
55. Schmutz J, Cannon SB, Schlueter J, Ma J, Mitros T, Nelson W, et al. Genome sequence of the palaeopolyploid soybean. Nature. 2010;463(7278):178–83. https://doi.org/10.1038/nature08670.
56. Schlueter JA, Lin JY, Schlueter SD, Vasylenko-Sanders IF, Deshpande S, Yi J, et al. Gene duplication and paleopolyploidy in soybean and the implications for whole genome sequencing. BMC Genomics. 2007;8(1):330. https://doi.org/10.1186/1471-2164-8-330.
57. Herdean A, Nziengui H, Zsiros O, Solymosi K, Garab G, Lundin B, et al. The Arabidopsis thylakoid chloride channel AtCLCe functions in chloride homeostasis and regulation of photosynthetic electron transport. Front Plant Sci. 2016;7:115. https://doi.org/10.3389/fpls.2016.00115.
58. Liu X, Pi B, Du Z, Yang T, Gu M, Sun S, et al. The transcription factor GmbHLH3 confers Cl−/salt tolerance to soybean by upregulating GmCLC1 expression for maintenance of anion homeostasis. Environ Exp Bot. 2022;194:104755. https://doi.org/10.1016/j.envexpbot.2021.104755.
59. Zhang T, Yu L, Chen Y, Zeng Y, Pi B, Liu X, et al. Physiological functions of the transcription factor *GmZAT10-1* gene involved in the salt stress adaptation in soybean. Plant Sci. 2025;355:112485. https://doi.org/10.1016/j.plantsci.2025.112485.

Publisher's Note